Geomorphology 284 (2017) 175–190

Contents lists available at ScienceDirect

Geomorphology

journal homepage: www.elsevier.com/locate/geomorph

Sedimentation close to the active Medlicott Wadia Thrust (Western Himalaya): How to estimate climatic base level changes and tectonics

V. Vignon [a], J.-L. Mugnier [c,d,*], R. Vassallo [c,d], P. Srivastava [f], M.A. Malik [e], R. Jayangondaperumal [f], F. Jouanne [c,d], J.F. Buoncristiani [g], J. Carcaillet [a,b], A. Replumaz [a,b], H. Jomard [h]

[a] Univ. Grenoble Alpes, ISTerre, F-38041 Grenoble, France
[b] CNRS, ISTerre, F-38041 Grenoble, France
[c] Université de Savoie-Mont-Blanc, ISTerre, F-73376 Le Bourget du Lac, France
[d] CNRS, ISTerre, F-73376 Le Bourget du Lac, France
[e] Department of Geology, University of Jammu, India
[f] Wadia Institute of Himalayan Geology, Dehra Dun, India
[g] BioGeoscience, University of Burgundy, France
[h] Institut de Radioprotection et de Sûreté Nucléaire (IRSN), France

ARTICLE INFO

Article history:
Received 14 March 2016
Received in revised form 26 June 2016
Accepted 29 July 2016
Available online 6 August 2016

Keywords:
Strath terraces
Allostratigraphy
Himalaya
Out-of-sequence thrust
Growth fault

ABSTRACT

The Medlicott-Wadia Thrust (MWT) is one of the major active out-of-sequence thrusts in the Himalaya. Studies on Quaternary terraces in its vicinity have been performed using sedimentological, geomorphic and geochronological methods. We focus on the Riasi zone, south of the Pir Panjal range, in the Jammu and Kashmir region of India. The sedimentary units of Quaternary landforms have been mapped as a function of their location with respect to the thrust faults, their relative chronology, and their lithology. Three aggrading sedimentary units, five thin units above strath surfaces at the footwall of the fault system, and seven thin units above strath surfaces at its hangingwall are identified. The terraces have been dated by combining Optically Stimulated Luminescence (OSL) on fine-grained deposits and cosmogenic-nuclide dating (^{10}Be) on sandstone pebbles sampled along depth profiles throughout the alluvial units. Three major allostratigraphic units were defined with upper surface ages estimated at ~4, ~15, and 36 ± 3 ka; the two older allostratigraphic units are encased terraces at the hangingwall but superposed sedimentary units at the footwall. They are related to phases of elevation of the river level (respectively 30 and 60 m) at ~36–38 and 14–15 ka and to a phase of extensive lateral incision before ~4 ka. These units present vertical offsets induced by the MWT of 50, 190, and 375 m, respectively. By taking the aggradation/incision rates at the footwall of the MWT into account, we found that the uplift of the hangingwall remains uniform since 36 ka, with a value of ~10 mm/yr. Therefore, the aggradation/incision events observed in the Riasi area cannot be ascribed to variations in the tectonic rates and are most likely driven by climatic fluctuations. The high uplift rate is possibly local and related to the Chenab recess, which affects the Himalayan frontal structure. Our results indicate that the MWT is an active growth fault, and one of the main emergences of the active Indian/Asian plate boundary in Western Himalaya.

1. Introduction

In a mountain belt, sediment flux results from the change in the shape of the landscapes. The latter is a critical interface between two interacting systems: an internal system driven essentially by tectonic fluxes of rock, and an external system dominated by the effects of climate (e.g. Allen, 2005). Recently, methodological progress in quantifying the rates of the surface processes as well as revived interest in the couplings between surface processes, tectonics and climate, have made it possible to renew our understanding of the interactions between sedimentation and tectonics (e.g. Castelltort et al., 2015). In Himalaya, the changes in the levels of the rivers are controlled by a combination of local tectonics, regional tectonics and climatic fluctuations (Lavé and Avouac, 2001). In some areas, a succession of aggradation, lateral and/or vertical incision events leads to a complex sedimentary pattern (e.g. Bookhagen et al., 2006). The study of this pattern results in a better understanding of the interactions between sedimentation and tectonics and better knowledge of the climatic evolution and active tectonics of the Himalaya (e.g. Dortch et al., 2011).

Himalayan tectonics are mainly controlled by large earthquakes of Mw ~8 that usually rupture the Main Frontal Thrust (MFT) at the front of the range (Kumar et al., 2006; Jayangondaperumal et al.,

* Corresponding author at: Université de Savoie-Mont-Blanc, ISTerre, F-73376 Le Bourget du Lac, France.
E-mail address: jean-louis.mugnier@univ-savoie.fr (J.-L. Mugnier).

http://dx.doi.org/10.1016/j.geomorph.2016.07.040
0169-555X/

2013; Mugnier et al., 2013). Nonetheless, the 2005 Mw 7.6 earthquake in Kashmir ruptured an out-of-sequence thrust 150 km north of the MFT (Kaneda et al., 2008). This thrust is part of the Medlicott-Wadia Thrust (MWT) that continues over more than 200 km toward the south-east (Thakur et al., 2010). The pattern of historical earthquakes leaves significant seismic gaps along the Himalayan arc (Seeber and Armburster, 1981) and a major gap is located between the 2005 Kashmir earthquake and the 1905 Kangra earthquake (Hussain et al., 2009; Thakur and Jayangondaperumal, 2015).

This study focuses on a segment of the MWT within this seismic gap (Fig. 1). The geomorphological and sedimentological signatures of earthquakes that rupture the surface north of the front in the Himalayan belt are difficult to recognize (Mugnier et al., 2005) due to the steep relief, the strong erosion and the complex sedimentation/incision pattern that affect the rivers within the chain. The quantification of the processes in this zone is therefore delicate and could lead to variable results. For example, two estimations of the MWT tectonic rates have been published recently (Vassallo et al., 2015; Gavillot et al., 2016); the study of Vassallo et al. (2015), which focused on the geometry of a local river alluvial fan, found an ~11 mm/yr shortening whereas the study of Gavillot et al. (2016), which did not take the influence of the aggradation events into account, found that the shortening would only be 6–7 mm/yr.

The aim of this paper is to estimate local tectonics, regional tectonics and climatically controlled base level changes in the sediment record close to this active out-of-sequence thrust. To do this, we propose a strategy that simultaneously incorporates sedimentological, geomorphological, geochronological and topographical methods. By separating the tectonics from the climatic signal in the sediment deposited in the Riasi area, a precise quantification of the tectonic activity of the MWT will be performed. This will allow for a better assessment of the seismic hazard in the seismic gap of the Western Himalaya.

To define the incision story in the vicinity of the thrust and to separate the role of local tectonics from the change in the river level, our approach combines the following aspects:

- Sedimentary units are characterized by their lithology (source origin) and their structural location (in the hangingwall or footwall of the main thrust);

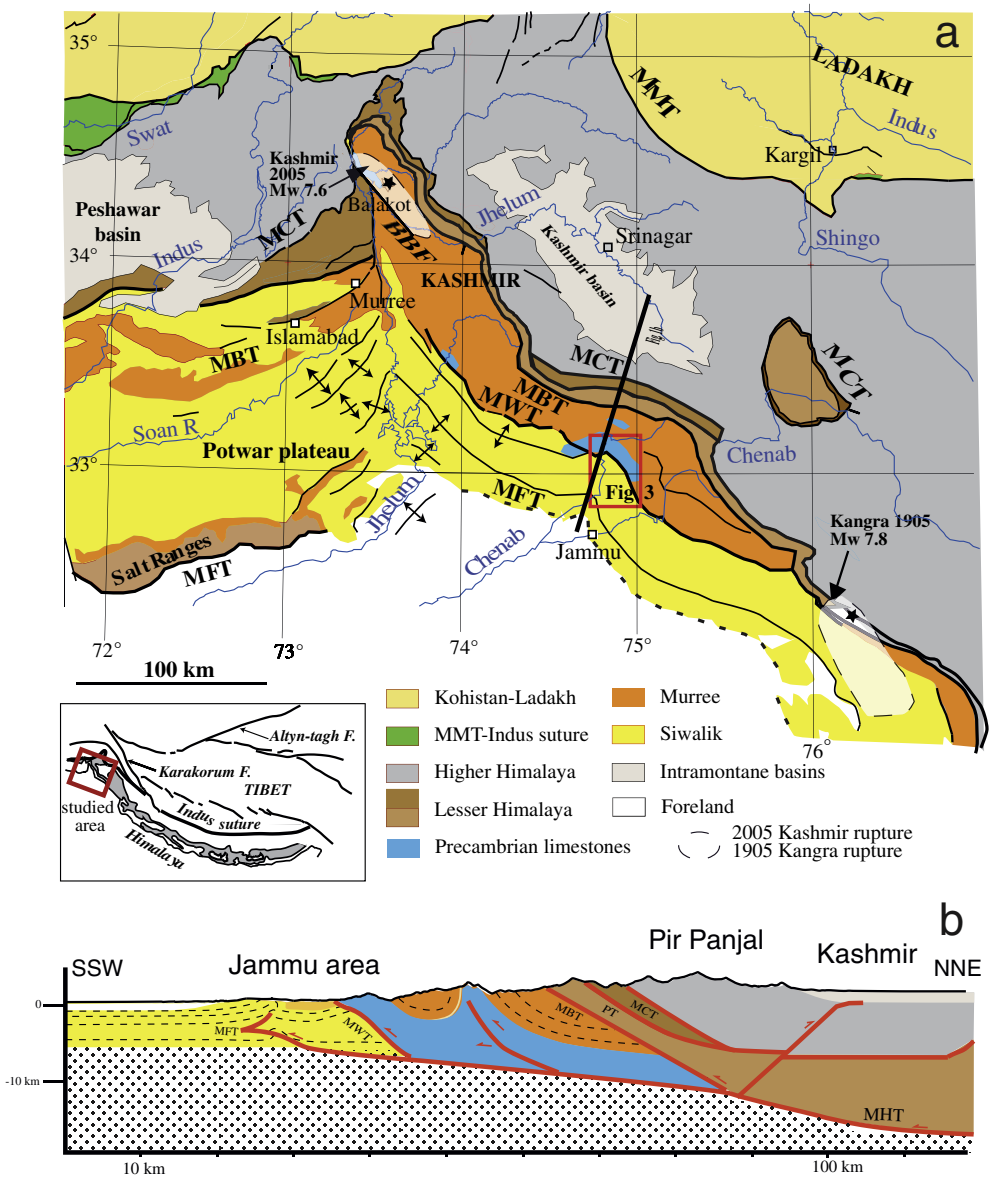

Fig. 1. (a) Geological map of the northwest Himalaya (modified after Pêcher et al., 2008) showing the rupture zones (dashed, shaded ovals) and epicentres (black stars) of the 1905 Kangra and 2005 Kashmir earthquakes. MMT: Main Mantle Thrust; MCT: Main Central Thrust; MBT: Main Boundary Thrust; MWT: Medlicott-Wadia Thrust; MFT: Main Frontal Thrust. (b) Cross-section through the Kashmir and Jammu area (location in panel a); MHT: Main Himalayan Thrust; PT: Pir Panjal Thrust.

- Relative ages of the hangingwall and footwall units are defined separately and deduced either from the stratigraphic superposition of the sedimentary units or from abutments that separate the top surfaces of encased terrasses (e.g. Burbank and Anderson, 2001);
- Optically Stimulated Luminescence (OSL) and in situ ^{10}Be cosmogenic dating were performed together to estimate the age of the alluvial constructions;
- Numerical dating allows a correlation between some footwall and hangingwall units and to define an allostratigraphic scheme (Hughes, 2010);
- Topographic measurements of the allostratigraphic units (mapping, thickness, altitude of their boundaries) quantify the incision. They are based on DGPS kinematic methods, total station topographic leveling and ASTER GDEM (see online Supplementary material, Appendix 1).

The vertical throw of the faults and the local change in the river levels are then deduced from the difference between the footwall and hangingwall incision story.

2. Approaches and methods

2.1. Relationships between the alluvial units, incision and quantification of active tectonics

Sedimentary units deposited above active thrusts record their tectonic activity. Two end-member syntectonic sedimentary units are classically considered: 1) terrace surfaces, considered to be passive markers, provide an estimate of the vertical throw associated with fault scarps (e.g. Hetzel et al., 2002) or the uplift at the scale of anticline structures (e.g. Nissen et al., 2009); 2) syntectonic strata deposited above growing structures (e.g. Vergés et al., 1996) record the interplay between the tectonics and sedimentation rates. In a continental context, numerous cases are between these two end members: the base level change influences sedimentation in a complex manner, depending the respective value of the base level change and the uplifts of the different structural zones (e.g. Huyghe and Mugnier, 1994). In the following, the relationships between incision, uplift and the change in the river level are detailed in order to define an allostratigraphic scheme (Hughes, 2010) for the formation of the terraces and syntectonic strata units in the vicinity of an active out-of-sequence thrust. Allostratigraphy uses bounding discontinuities to subdivide sedimentary successions and includes lateral lithologic variations within a single stratigraphic unit; the bounding discontinuities are faults, unconformities, disconformities, or the present-day land surface; in some instances, prolonged surface exposure may be recorded by palaeosols forming allostratigraphical boundaries (Hughes, 2010).

Incision may cause the abandonment of geomorphic surfaces, creating discontinuities at the top of a sedimentary unit. Within a fixed reference frame (here the Indian plate), incision is written as a function of tectonic uplift and the change in the river profile (adapted from Lavé and Avouac, 2001):

$$I_{(x,t)} = U_{(x,t)} - B_{(x,t)} \quad (1)$$

where I is incision; U is tectonic uplift and B is the change in the river level. $I_{(x,t)}$, $U_{(x,t)}$ and $B_{(x,t)}$ are considered at location x and at time t (Fig. 2a). By definition, the vertical throw of a fault (V) is:

$$V = U_{(h,t)} - U_{(f,t)} \quad (2)$$

with (h, t) and (f, t) referring to the hangingwall and the footwall, respectively. Two equations can be derived from applying Eq. (1) to a terrace (top of a sedimentary unit) that extends above the footwall and hangingwall of a thrust:

$$I_{(h,ti)} = U_{(h,ti)} - B_{(h,ti)} \quad (3)$$

$$I_{(f,ti)} = U_{(f,ti)} - B_{(f,ti)} \quad (4)$$

with $_{(h,ti)}$ and $_{(f,ti)}$ referring to the abandonment of a terrace since "$_{ti}$" years in the hangingwall and footwall, respectively.

The contribution of the horizontal motion component is negligible when the channel gradient is small (Kirby and Whipple, 2001); in

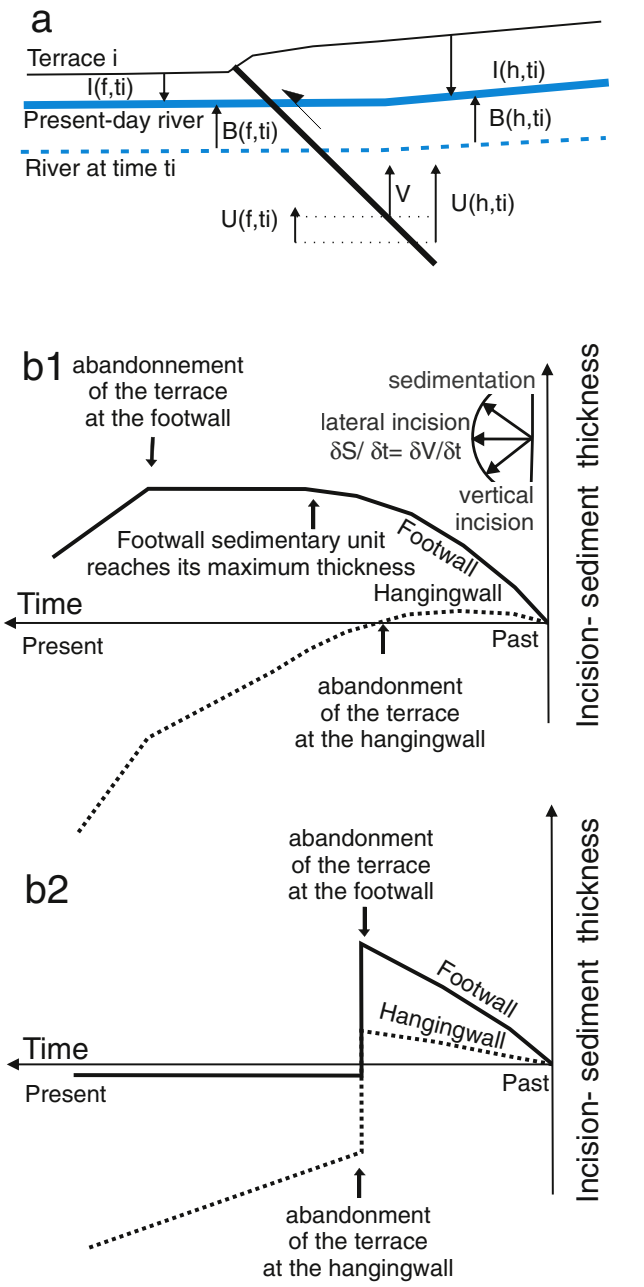

Fig. 2. (a) Sketch of a terrace passively deformed by a thrust and definition of the parameters: V (vertical motion of the fault); U (tectonic uplift); I (incision); B (base level change); h and f are location at the hangingwall and footwall, respectively; and t_i time of abandonment of the terrace. (b) Deposition/incision history of the hangingwall and footwall for a constant vertical motion of the fault; b1) for a progressive decline in the sedimentation rate δS/δt; (b2) for an instantaneous decrease in the sedimentation rate.

addition, the change in the river level induced by a change in the channel gradient over a short horizontal distance is also negligible; therefore:

$$B_{(h,ti)} \approx B_{(f,ti)} \quad (5)$$

From the difference between Eqs. (3) and (4) and substitution in Eq. (2):

$$V = I_{(h,ti)} - I_{(f,ti)} \quad (6)$$

This implies that, even for a terrace level that has been synchronously abandoned, and that forms a passive marker, the activity of a thrust needs to be deduced both from the hangingwall and footwall terrace position and not only from the hangingwall terrace. The difference of incision between the hangingwall and the footwall for such an isochronous surface only reflects the local tectonic activity and is unaffected by regional uplift or changes in the base level of the river bed.

A comparison between the footwall and hangingwall is also necessary in the case of syntectonic alluviation. This type of alluviation is defined by its sediment thickness S and its sedimentation rate $\delta S/\delta t$ at the footwall of a thrust; S is taken as negative in the case of incision. The evolution of the hangingwall of a thrust, which slips at a rate of $\delta V/\delta t$, is the following (Fig. 2b1):

- Sedimentation occurs if $\delta S/\delta t > \delta V/\delta t$,
- Vertical incision affects the hangingwall block if $\delta S/\delta t < \delta V/\delta t$.
- Lateral incision and large strath surface development occur if $\delta S/\delta t = \delta V/\delta t$. The development of strath terraces could also be linked to extreme flooding events but in this case, their extent is expected to be smaller.

Thus, if alluviation at the footwall of a thrust might be expressed by strath surface formation at the hangingwall of an active thrust, the abandonment of the hangingwall and footwall surfaces are not necessarily synchronous: the abandonment of the hangingwall surface occurs as soon as the sedimentation rate $\delta S/\delta t$ is less than $\delta V/\delta t$ and precedes the deposition of the upper part of the footwall unit. Furthermore, footwall surface abandonment could largely post-date that of the hangingwall: in the case of a steady-state river profile (with no long-term change in sedimentary thickness at the footwall), extreme flooding events may still remobilize the top of the sediments as long as no incision greater than the flooding height affects the footwall units. The lag between the abandonment of the footwall and hangingwall is illustrated in Fig. 2b1 in the case of a linear decline in the hangingwall sedimentation rate. Nonetheless, abandonment of terraces at the hangingwall could be synchronous with the fall in the footwall sedimentation rate if the decrease is nearly instantaneous and leads to a vertical incision of the footwall (Fig. 2b2). As climatic variations induce rapid increases in the river transport capacity that are amplified by a positive feedback between the discharge and channel gradient (Simpson and Castelltort, 2012), they drive rapid abandonment and the incision of large terraces (e.g. Bookhagen et al., 2005). It is therefore inferred that, for a region affected by a rapid climatic variation, abandonment of terraces is synchronous between the footwall and hangingwall of a thrust. Therefore, in the vicinity of a large thrust, the lateral variation from the strath terraces to fill terraces is included within the same allostratigraphic unit bounded at its top by the terrace tread. An allostratigraphic description, based on this assumption, is used below to quantify the incision/sedimentation rates and the tectonic activity.

2.2. Dating morphologic markers

In the studied area, surface dating by terrestrial cosmogenic nuclides (TCN, e.g. Brown et al., 1998) is challenged because erosion does not result in the full preservation of terrace features, which are submitted to strong subtropical rainfall events and affected by agriculture. OSL dating of the deposits (e.g. Aitken, 1998) may also biased by partial bleaching of the transported sediments before alluviation (e.g. Srivastava et al., 2009). These dating methods refer to different geomorphological processes: abandonment of the surface by the river for TCN and an alluviation event for OSL. Numerical dating of terraces is subject to great uncertainty due to the uncertainties linked to each dating technique and the time lapse between the abandonment of the top surface and the end of the alluviation phase. Nonetheless, in this context, we consider that the delay between the geomorphological processes is negligible or within age uncertainties (see the discussion above). Therefore, both dating methods have their own limitations but together, they provide some strength that the ages they yield are reliable.

2.2.1. ^{10}Be cosmogenic dating

The in situ-produced ^{10}Be concentration is a function of the time of exposure and has been the terrestrial cosmogenic nuclide most commonly used over the last two decades to quantify the age of abandonment of morphological markers (e.g. Bierman et al., 1995; Anderson et al., 1996; Vassallo et al., 2015). A minimum age of a terrace is provided by the present-day surface deposits (Brown et al., 1998). Boulders well-encased in the alluvial matrix at the surface were sampled to reduce the risk of their post-depositional remobilization; samples were extracted from the upper part of the boulders and were less than 5 cm thick.

Profiles were also sampled at a depth of several meters on fresh exposures comprised of cliffs related to landslides or road trenching; they can be used to estimate the post-depositional denudation of the surface and the ^{10}Be inheritance from prior terrace formation (e.g. Hancock et al., 1999). The depth attenuation profile of the ^{10}Be concentration is linked to the post-depositional denudation and the best attenuation profile was calculated using the inversion procedure defined by Hidy et al. (2010). The inheritance was estimated from the deepest sample, which is the one that is the most protected from cosmogenic rays (Anderson et al., 1996; Brown et al., 1998). Sand samples would furnish a natural statistical approach of the stochastic distribution of the inheritance (e.g. Brown et al., 1995), but the size of the clasts also influences the inheritance (Vassallo et al., 2011); therefore, we chose to collect cobbles with sizes close to those of the surface samples. In order to minimize the dispersion of the ^{10}Be inheritance linked to variable river transport velocities, we collected pebbles provided by the closest upstream source: the Murree sandstones that crop out less than twenty kilometres upstream.

The methods and parameters used to interpret the TCN data are not yet standardized and continue to evolve as the result of ongoing work aimed at understanding the global and temporal distribution of production rates (Frankel et al., 2011). In the following, production rates were calculated as a function of altitude and latitude using the Cronus calculator (Balco et al., 2008) based on the scaling model of Lal (1991) and Stone (2000), with a production rate of 4.5 ± 0.3 ^{10}Be At/g/a at sea level and high latitude. Geomorphic shielding factors were calculated following Dunne et al. (1999). Beryllium oxide targets were extracted following the chemical procedure of Brown et al. (1991). The ^{10}Be targets were measured at the French National Accelerator Mass Spectrometry facility ASTER (Arnold et al., 2010). Analytical uncertainties calculated for ^{10}Be/^{9}Be include uncertainties associated with the AMS counting statistics, the AMS external error (0.5%), and the chemical blank measurement ($6.799 \pm 1.50 \times 10^{-15}$; $4.099 \pm 1.18 \times 10^{-15}$ for the 2008 and 2010 measurements, respectively). The measured ^{10}Be concentrations were normalized using a factor of 1.142 ± 0.039 (Middleton et al., 1993). The ^{10}Be concentrations were calibrated against NIST Standard Reference Material 4325 using its certified ^{10}Be/^{9}Be ratio of $(2.79 \pm 0.03) \times 10^{-11}$. We used a ^{10}Be half-life of 1.387 ± 0.012 Ma (Chmeleff et al., 2010) and attenuation lengths of 150, 1500 and 5300 g/cm^2 with associated relative contributions to

the total production rate of 97.85%, 1.50% and 0.65% for neutrons, slow muons and fast muons, respectively (Braucher et al., 2003).

2.2.2. Optically Stimulated Luminescence

The OSL technique relies on the premise that, before deposition, geological luminescence stored in the minerals is zeroed by day light exposure during erosion and transport. After burial, the exposure to daylight ceases and a re-accumulation of luminescence occurs due to irradiation from ambient radioactivity. Analysis of this luminescence and the ambient radiation environment provides the age of the burial event (Aitken, 1998). Nonetheless, fluvial sediments in the Himalaya are generally deposited under high-energy turbulent conditions and may be inhomogeneously zeroed (Srivastava et al., 2009). Numerous OSL analyses on Himalayan sediments, based on the single-aliquot regeneration (SAR, from Murray and Wintle, 2000) protocol, were performed (Srivastava et al., 2013a,b *and references therein*; Mehta et al., 2014). It was found that the effects of incomplete bleaching can be countered by measuring ~30 aliquots, by reducing the aliquot size and by only taking the lowest palaeodoses into account in the age estimation, as already proposed by Galbraith et al. (1999). In this paper, the least palaeodose is defined as the median of the lowest 20% of the palaeodoses and is used to calculate an age referred to in the following as the youngest OSL age. Furthermore, to optimize the accuracy of the dating, the sampled levels are those where the reset of the geological luminescence before sedimentation is expected to be maximized, i.e. levels mainly made up of fine grains in thin sedimentary horizons (see the discussion in the online Supplementary material, Appendix 2).

Sampling was carried out using opaque stainless steel pipes driven into sections preserved from any natural or anthropic reworking. Dating was carried out at the Wadia Institute of Himalayan Geology (Dehra Dun, India) using the technique developed by Srivastava et al. (2009). The uncertainty in the OSL age estimation arises from both the geochemical analysis uncertainties and modelling procedures; standard mathematical procedures built into the *Analysts* software (Duller, 2007) are used to propagate the effects of the uncertainties in the age estimation.

3. Geological and geomorphological results

3.1. Geology of the area

The Himalayan tectonics, due to the India-Eurasia convergence, produces active deformation on the south-vergent thrusts. Within the Jammu-Kashmir area, the shortening reaches ~16 mm/yr (Jouanne et al., 2014). Nonetheless, this area has not experienced any major seismic events since the Mw > 7 Srinagar earthquake in 1555 AD (Ambraseys and Douglas, 2004). Thus it is a potential spot for a future great earthquake rupture. The MWT extends from the area affected by the 2005 Kashmir earthquake to the one affected by the 1905 Kangra earthquake (Hussain et al., 2009; Fig. 1). The MWT is located on the southern flank of the Pir Panjal range between the Kashmir basin and the Indian plain (Fig. 1 from Pêcher et al., 2008). The study focuses on a segment of the MWT close to its intersection with the Chenab River, where the MWT is usually referred to as the Riasi thrust (Thakur et al., 2010). The hangingwall of the MWT is mainly formed by the Palaeocene to Miocene Murree formation. This is a fluvial formation consisting of fine-grained sandstones, siltstones, and purple to brown shales. In the Chenab area, the Murree formation overlies Eocene and Precambrian limestones (Gansser, 1964; Krishnaswamy et al., 1970) and the hangingwall of the Riasi thrust is formed from these limestones (Fig. 1). The relief associated with this lithology rises to more than 2000 m.

The foothills between the plain and the MWT rise to ~1000 m. They stand above the frontal anticline which folds the foreland basin infilling deposits (Mugnier and Huyghe, 2006), known as Siwalik. The Siwalik group consists of a ~5 km pile of fluvial deposits (Mugnier et al., 1992). The frontal structure has been active since at least 1.7 Ma as indicated by the development of an unconformity above tilted Siwaliks at the southwestward termination of the frontal anticline (Johnson et al., 1979), close to the Jhelung River.

The main structures are locally affected by a recess (Marshak, 2004) where the Chenab flows. In the recess, the footwall of the MWT is composed of fluvial sediment deposited above the Siwaliks (Fig. 3). The

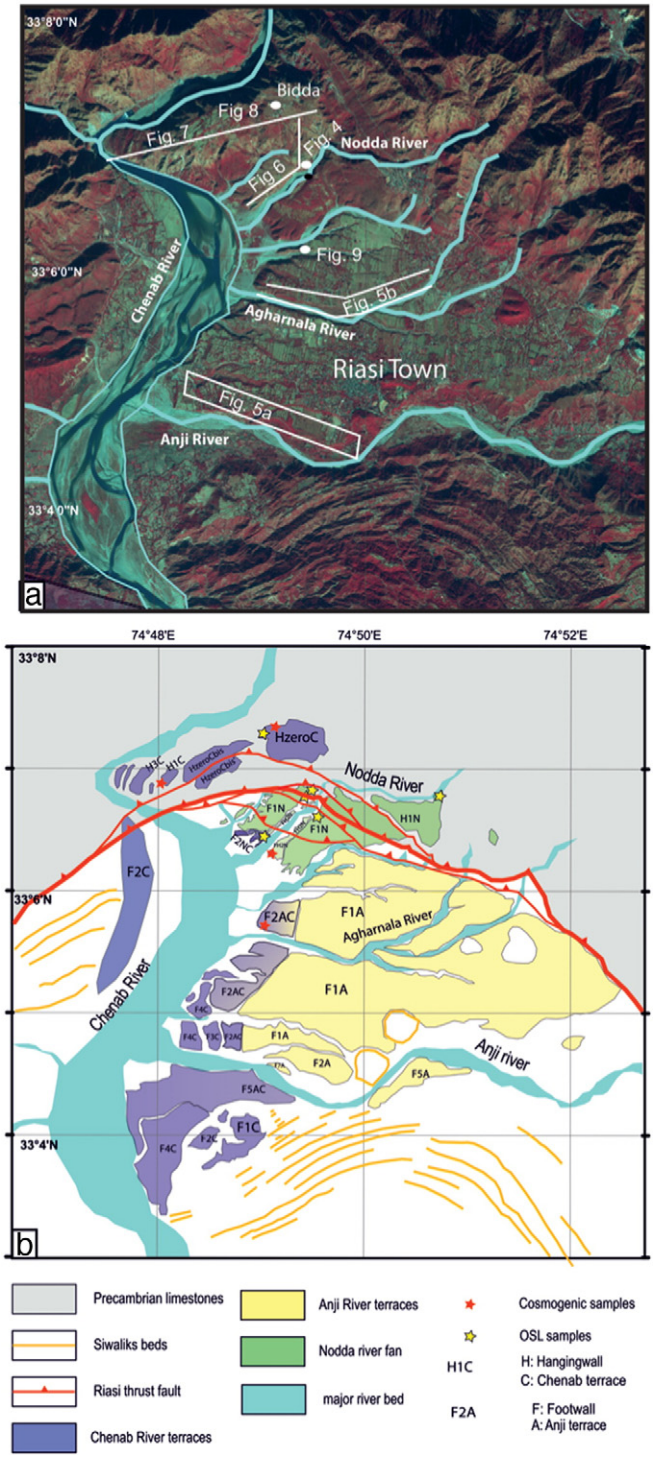

Fig. 3. Morphotectonic map of the Riasi area. (a) Satellite image (SPOT) of the study area with the location of the other figures. (b) Morphotectonic interpretation. Sedimentary unit names depend on: (1) the position in relation to the Riasi thrust (i.e. F: Footwall; H: Hangingwall); (2) relative altitude above the present-day river bed (0 for the highest, 5 for the lowest). Note that two different numbering systems were used for the footwall and hangingwall of the thrust. (3) The river at the origin of the deposition (i.e. C: Chenab; A: Anji; N: Nodda).

MWT is formed here by a splay that grows during sedimentation. Vassallo et al. (2015) described five branches of this splay but only two of them were recognized by Gavillot et al. (2016). Local names are used for the different branches, from north to south: the Pilar and Spring faults affect the limestone sheet, the Tea fault is at the base of the limestone sheet, whereas the Scorpion and Rain faults affect the Cenozoic deposits.

3.2. River catchments and associated deposits in the Riasi area

The quaternary sedimentary units of the Riasi area reflect the lithologies that crop out in the catchments of the Chenab, Anji and Nodda Rivers and their geomorphological characteristics.

3.2.1. Chenab fluvial terrace

The Chenab River flows from north to south draining a catchment area of more than 11,500 km^2. It begins in the Higher Himalaya and crosses various geological units: volcanic traps, granites, quartzites, Murree sandstones, and Precambrian limestones.

The Chenab River builds fluvial terraces and the sediments of the Chenab river terraces are typically well-sorted, well-rounded, pebble to boulder matrix conglomerates (Fig. 4a2). These deposits display nearly horizontal bedding to large-scale channel bedding with palaeocurrent-imbricated cobbles. Furthermore, sands frequently form overbank deposits (Fig. 4a1).

3.2.2. Anji alluvial fan

The Anji River, a tributary of the Chenab River, flows from east to west. Its catchment area is roughly 114 km^2 and composed of Precambrian limestones and Murree sandstones.

The Anji River builds an alluvial fan-terrace (Fig. 4b) with the top sequence displaying crude planar bedding (30 cm to 1 m). The Anji alluvial fan consists of sub-angular to sub-rounded pebbles in a poorly- to moderately-sorted coarse sand matrix conglomerate with clast imbrications. These deposits display sparse channels infills (up to 1.5 m high and 5 m wide) of cobble to boulder matrix conglomerates, with planar cross-bedded stratifications. This formation has been referred to as the Anji Khad terraces by Nawani et al. (1982).

3.2.3. Nodda alluvial fan

The Nodda catchment is composed exclusively of Precambrian limestones. The Nodda River catchment area is roughly 5 km^2 and the river has built an alluvial fan in the vicinity of the Chenab River. Eastwards, other small tributaries draining the Precambrian limestones also built thick alluvial fans at the footwall of the thrust. These are indistinctly

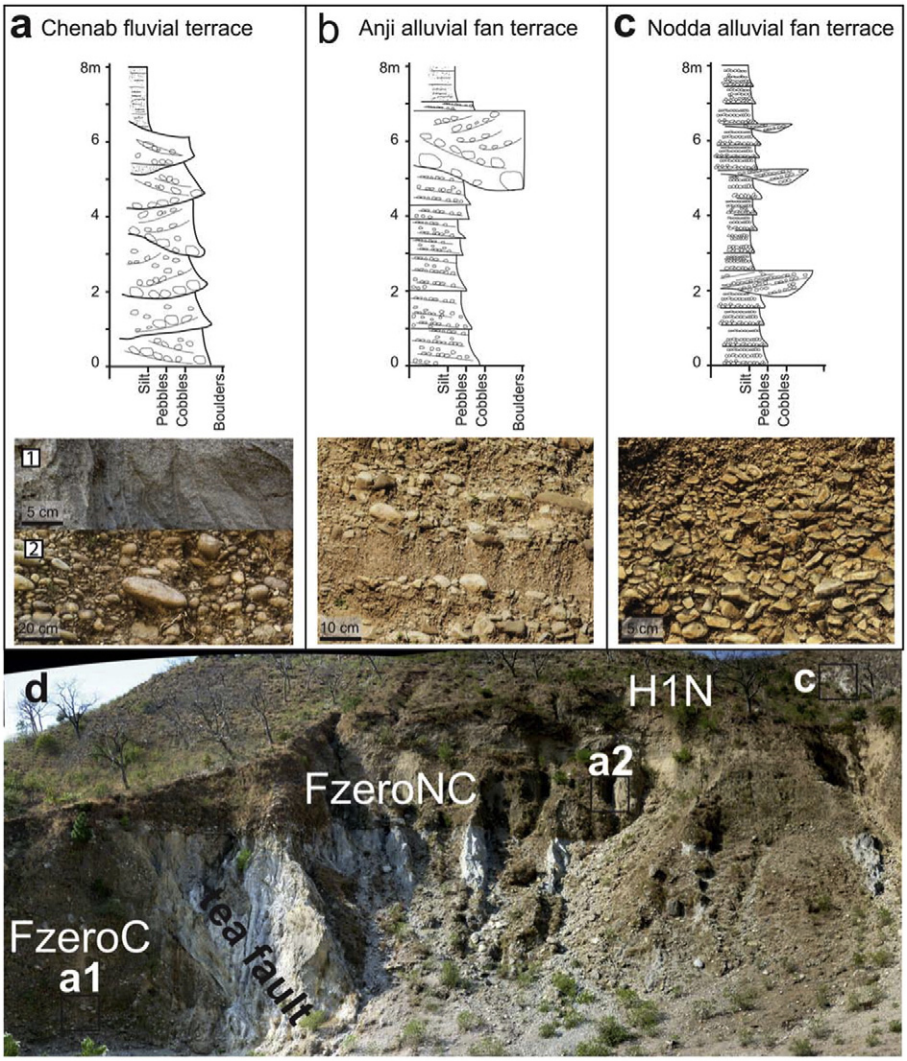

Fig. 4. Synthetic logs and associated facies illustrations: (a) Chenab River terrace (HzeroC terrace); a1) for coarse sand; a2) for pebbles. (b) Anji alluvial fan (F1A terrace). (c) Nodda alluvial fan (F1N terrace). Note the different scales for the three illustrations. (d) Sedimentary units observed along the Nodda River in the vicinity of the Tea fault branch of the Riasi thrust. a1, a2 and c are located in the FzeroC, FzeroNC, F1N units respectively and refer to the location of the above facies illustrations.

described as the Vaishno Devi Formation by Thakur et al. (2010) or the Sirban formation by Gavillot et al. (2016).

The Nodda alluvial fan deposit (Fig. 4c) is composed of tabular sequences, exhibiting fining-up, planar bedding (40 cm to 1 m thick). These deposits consist of angular to sub-angular pebbles and well-sorted clast-supported conglomerates made up of Precambrian limestone. The Nodda fan displays small channels (up to 40 cm high and 1.5 m wide) of pebble matrix conglomerates with basal cobble lags, and medium-scale planar cross-bedded stratifications.

3.3. Mapping of the Quaternary sedimentary units

SPOT satellite images, together with field mapping and a topographic survey, were used to map the fluvial terraces and alluvial fans in the Riasi area.

The proposed mapping of the alluvial surfaces (Fig. 3b) takes into account: (1) the position with respect to the Riasi thrust (H for Hangingwall; F for Footwall); (2) the relative elevation of the terrace in the vicinity of the Chenab River, with respect to the present-day river (zero for the highest; 5 for the lowest); and (3) the origin of the sediment (C for Chenab; A for Anji; N for Nodda or Agharnal and double letters for inter-bedded sediments).

3.3.1. Footwall terraces

The most extensive surface is F1A. This surface is 7 km long and widens from east to west to reach 4 km at its broadest. Its slope is nearly constant (4% toward the west) (Fig. 5b) and is steeper than the present-day 2% slope of the Anji River. The sediments usually display typical Anji facies, but limestone predominates to the north and the Anji sediments are interbedded to the west with Chenab deposits.

The F1A deposits are more than 60 m thick in their north-western part. Southward, F1A thins progressively above the north limb of the frontal anticline and it evolves laterally into the F1C strath terrace formed by a 12 m thick unit. This lateral evolution is related to the frontal anticline development and uplift (Vassallo et al., 2015). F1A is therefore a large fan of the Anji River that laterally interacted with other tributaries and developed between two uplifted zones: the hangingwall of the Riasi thrust and the frontal anticline.

F2AC is a fill-cut terrace in F1A and its surface dips southward. The sedimentary sequence of this unit is less than 4 m thick and it locally displays superposed channel infills from the Anji and Chenab rivers.

F3C, F4C, F5A and F5AC are the lowermost strath terraces, encased in the FA1 fan along the Chenab and Anji river beds (Fig. 5a).

3.3.2. Nodda River units developed above the Riasi thrust

The Nodda River alluvial fan (F1N, Fig. 3) developed above the Rain fault, Scorpion fault, Tea fault and Spring fault. Downstream, where the fan is more than 50 m thick, the Nodda and Anji river sediments are interbedded at the boundary of the F1N and F1A fans. The F1N fan has an average slope of 5 ± 1% toward the south, which locally increases to almost 30° at two tectonic scarps above the Scorpion and Rain faults (Fig. 6).

In the upper part of the F1N fan, on the side of the present-day Nodda River canyon, the sediments of the palaeo-Nodda River onlap the flanks of a canyon previously incised in the limestone.

Upstream, the fan is cut by the Pilar fault. The dating results (see Section 4.2.2) suggest that the apex of the fan, is deposited synchronously with the rest of the fan and preserved at the hangingwall of the Pilar fault; it is therefore called H1N. The upper part of this fan was not distinguished from the regional Sirban unit by Gavillot et al. (2016), while this is the case in the study by Vassallo et al. (2015). The slope at the apex is more than 10%.

A cut and fill terrace (F2N) was developed within the Nodda fan. It widens downstream and its termination merges westward with the fill-cut terrace (F2NC) deposited by the palaeo-Chenab River. At its southern termination, F2NC lies 50 m above the Chenab River and 10 m below the surface of F1N.

Two units are located beneath the sediments of the F1N Nodda fan, mainly outcropping along the Nodda River gorge (Fig. 4d). The FzeroNC unit is characterized by pebbles and sands rich in micas, corresponding

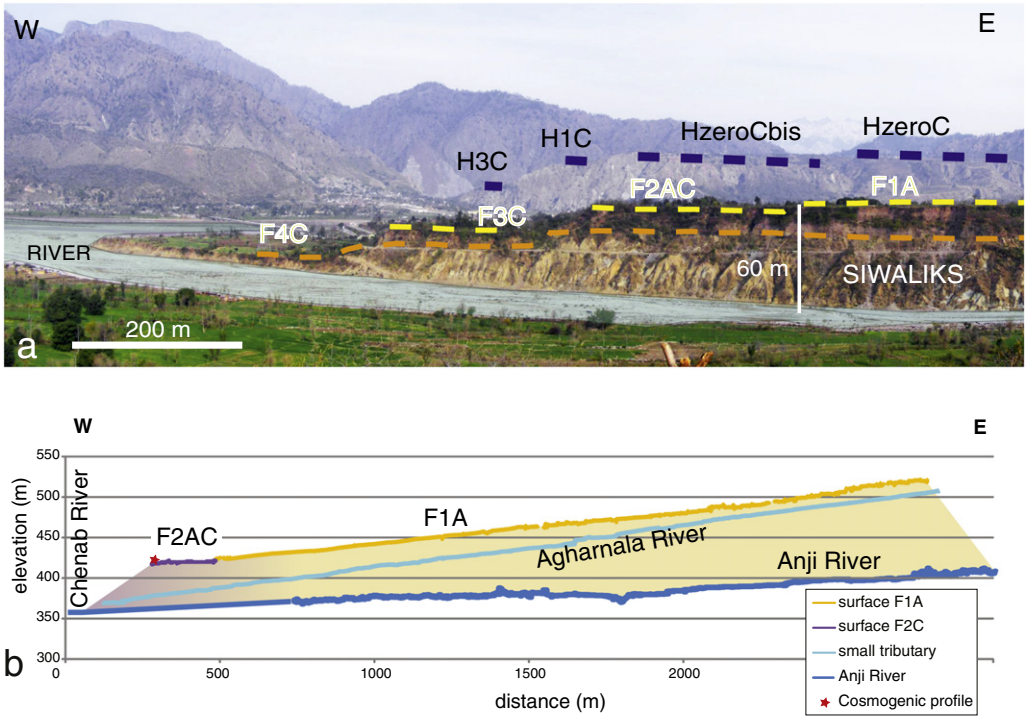

Fig. 5. The footwall terraces of the Anji and Chenab Rivers. See Fig. 3a for location. a) Panoramic view of terraces F1A to F4C (looking north); orange dashed line for the top of Siwaliks, yellow dashed lines for the footwall surfaces and blue lines for the distant hangingwall terraces. At its lower edge, F1A is located ~60 m above the river (vertical white bar). b) Comparison of the E–W profiles (measured by kinematic DGPS) along F2AC, F1A, Anji River and a small tributary (Agharnala River). The red star locates one of the ^{10}Be sampling sites.

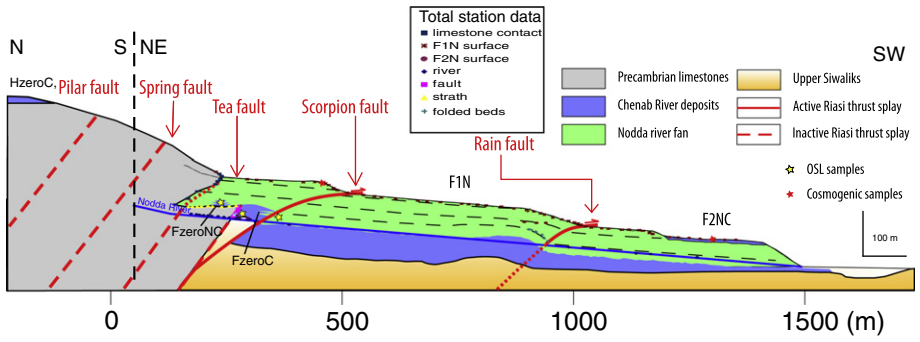

Fig. 6. Cross-section of the Nodda fan F1N and Riasi thrust splay (right bank of the Nodda River, location in Fig. 3a. Note the change in the orientation of the section). Total station data are projected along the lower portion of the cross-section.

to Chenab deposits, interbedded with limestone conglomerates supplied by the Nodda River. The upper boundary of the FzeroNC unit is defined on the western side of the Nodda River by the top of the highest overbank deposits formed of micaceous sand. It is also observed in the core of the Rain fault anticline (Fig. 6).

The FzeroNC unit is deposited upon the limestone and its lower boundary is formed by a rather planar strath surface (Fig. 4d). The FzeroNC unit seals the Tea fault located between the Chenab sediments and limestones and lies above the FzeroC deposits located at the footwall of the Tea fault. The FzeroC unit was deposited by the Chenab

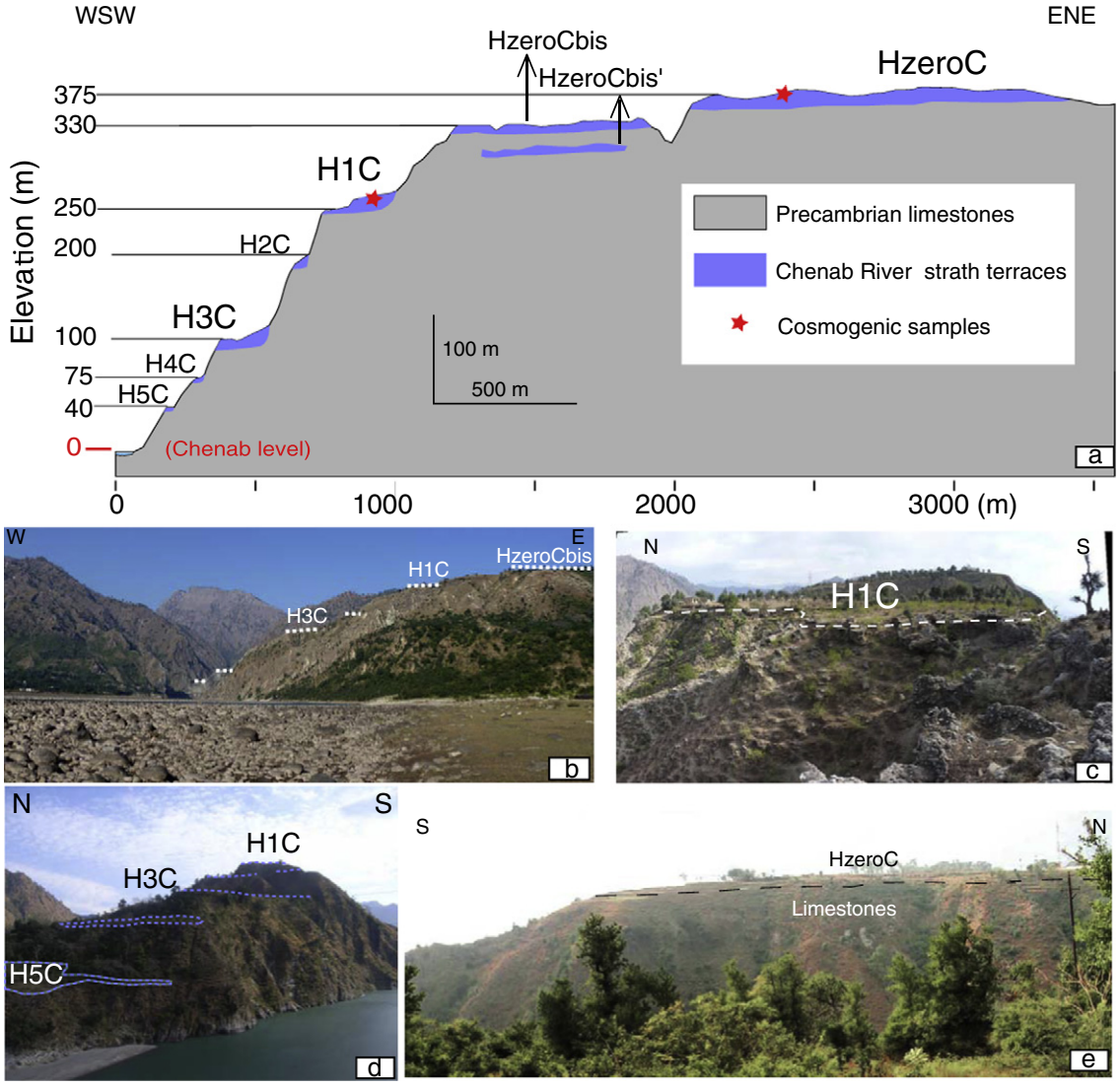

Fig. 7. (a) Cross-section through the Chenab strath terraces at the hangingwall of the Riasi thrust (vertical axis exaggerated). The altitude of the terraces is measured in reference to the Chenab River level. (b), (c), (d), and (e) are detailed pictures of the hangingwall terraces.

River above an erosional surface at the top of Middle Siwaliks, and the total thickness of the FzeroNC and FzeroC units is ~30 m.

3.3.3. Chenab terraces at the hangingwall of the Riasi thrust

In the hangingwall of the Riasi thrust, a meander in the Chenab River developed around a limestone spur (Fig. 3). Strath terraces directly overlie the limestone, at the top and on the western side of the spur.

The highest terraces (HzeroC and HzeroCbis) are 375 m and 330 m above the Chenab River, respectively (Fig. 7a). Thakur et al. (2010) previously confused HzeroC and H1N. Nonetheless, the Chenab terraces stand higher than the lower part of H1N fan, although HzeroCbis is lower than the apex of H1N: they are therefore older than this fan.

HzeroC is a 1 km wide flat surface varying in thickness from 4 to 15 m (Fig. 7e). HzeroCbis is located west of HzeroC and is locally offset (HzeroCbis′) by the Pilar fault.

At the western end of the spur, five less extended terraces (H1C to H5C) step toward the Chenab River (Fig. 7b and d). H1C (Fig. 7c) and H3C are locally covered by limestone gravel deposits from very small tributaries and are formed of thick units (more than 10 m) above the strath surfaces.

4. Dating results

4.1. ^{10}Be cosmogenic nuclides

Eighteen samples were analysed from four terrace levels for TCN dating (see Fig. 3b for location and Table 1 for results). The TCN content in the Chenab River sand was also measured to estimate the inheritance.

4.1.1. Upper terrace HzeroC

Seven samples of the HzeroC terrace were collected from a depth profile within a trench at the summit of the terrace (Fig. 8a). The depth attenuation was modelled (Fig. 8b) with the code developed by Hidy et al. (2010). We calculated (see the online Supplementary material, Appendix 3) that the minimum age, with the erosion assumed to be zero, is 21 ka (Fig. 8c). No erosion rate that exceeds 3.5 cm/ka gives a statistically acceptable fit (Fig. 8d). In this latter range of erosion rates, the age calculated for abandonment of the terrace ranges between 21 and ~100 ka, but is not characterized by a Gaussian distribution: the peak value is ~23 ka and the median value is ~37 ka. Therefore, it is considered that the abandonment ages range between 23 and 37 ka and the total erosion is between 0 and 1 m.

4.1.2. Terrace H1C

Two samples were collected from the surface of the H1C terrace (Fig. 7c). One sample experienced no significant exposure, presumably because of agricultural reworking of the soil. Therefore, the TCN age of this terrace is only estimated from the other sample that yields a minimum TCN age of 6.9 ± 1.6 ka; the age of the terrace would be 15.4 ka if erosion reached 3.5 cm/ka (maximum erosion on HzeroC from the TCN age modelling). Nonetheless, older ages cannot be ruled out because the H1C surface is subjected to hill-slope runoff and the erosion rate might be higher than for the HzeroC surface.

4.1.3. F2AC and F2NC sedimentary units

A depth profile was examined for terrace F2AC along a recent soil-sliding (Fig. 9a). It reveals considerable variations in the TCN concentration with depth (Fig. 9b). This scattering can be explained by episodes of lateral migration of the Anji and Chenab Rivers during the formation of the terrace, coupled with a strong variability of the ^{10}Be inheritance of the samples. The inheritance is catchment size-dependent (Yanites et al., 2009) and the mixing of sediments from the very different Chenab and Anji catchments would then induce a strong inheritance dispersion.

This concentration dispersion makes it unsuitable to compare the depth profile with an attenuation model. Therefore, only the surface samples were used to approximate the age of the terrace. The dispersion of the surface concentrations is linked to the inheritance and the lowest TCN concentration at the surface (sample JK-08-46 in Fig. 9b) is related to the lowest inheritance. The assumption of zero inheritance for this sample allows to calculate a maximum exposure age. This age is between 3.2 and 4.3 ka (heavy grey distribution in Fig. 9c) with a most probable value at 3.8 ka.

A few hundred meters to the north-west of the previous site, one Murree pebble was sampled on the surface of the F2NC terrace (sample JK-08-89 in Fig. 9b). A minimum age for this sample was calculated assuming no erosion and an inheritance equal to the concentration of the present-day Chenab sediments (Table 1). The modelled age is between 2.0 and 5.3 ka (Fig. 9c in light grey; see the online Supplementary material, Appendix 3), with a most probable value at 4.5 ka.

4.2. Optically-stimulated luminescence ages

Five samples were analysed for OSL dating: four along the Nodda River cut cliff section and one from the highest terrace. The U-Th-K concentrations, dosimetry, mean palaeodoses, and ages of the OSL samples are shown in Table 2. The palaeodose distribution, shine-down curves

Table 1
TCN dating of the terraces: sample location, topographic shielding (Dunne et al., 1999), ^{10}Be concentration and minimum ^{10}Be age assuming no erosion (see Section 2.2.1 for the methods and parameters used to interpret the TCN data; see online Supplementary Material, Appendix 3 for the estimation of the ages from the depth profiles).

Terrace	Sample ID	Latitude (±0.001) N°	Longitude (±0.001) E°	Altitude (m asl)	Height above Chenab River (m)	Shielding factor	Depth along profile (cm)	^{10}Be (10^4 at/g)	Error on ^{10}Be (at/g)	Denudation rate (mm yr^{-1})	Minimum age (ka)
Chenab Sand	JK.10.22	33.114	74.792	390	0	1	0	18,661	3590	0	–
HzeroC	JK.08.15	33.123	74.818	762	375	0.998	0	197,753	5804	0	21 ± 2
	JK.08.11	33.123	74.818	762	375	0.998	10	151,413	5370	0	
	JK.08.08	33.123	74.818	762	375	0.998	70	62,128	11,424	0	
	JK.08.07	33.123	74.818	762	375	0.998	125	14,987	2782	0	
	JK.08.05	33.123	74.818	762	375	0.998	280	7686	1686	0	
	JK.08.04	33.123	74.818	762	375	0.998	424	17,553	2086	0	
	JK.08.03	33.123	74.818	762	375	0.998	565	22,275	3242	0	
H1C	JK.10.18	33.114	74.8	650	250	0.993	0	60,074	4313	0	6.9 ± 1.6
	JK.10.19	33.114	74.8	650	250	0.993	0	9233	2308	0	
F2AC	JK.08.46	33.093	74.813	480	50	0.998	0	23,035	2152	0	3.8 ± 0.4
	JK.08.47	33.093	74.813	480	50	0.998	0	29,052	1965	0	
	JK.08.48	33.093	74.813	480	50	0.998	0	32,733	2106	0	
	JK.08.50	33.093	74.813	480	50	0.998	25	13,871	1300	0	
	JK.08.44	33.093	74.813	480	50	0.998	52	23,608	2988	0	
	JK.08.43	33.093	74.813	480	50	0.998	75	12,474	1058	0	
	JK.08.42	33.093	74.813	480	50	0.998	145	39,532	2897	0	
	JK.08.37	33.093	74.813	480	50	0.998	550	11,146	1942	0	
F2N	JK.10.89	33.106	74.819	480	50	0.998	0	34,602	5494	0	3.6 ± 1.6

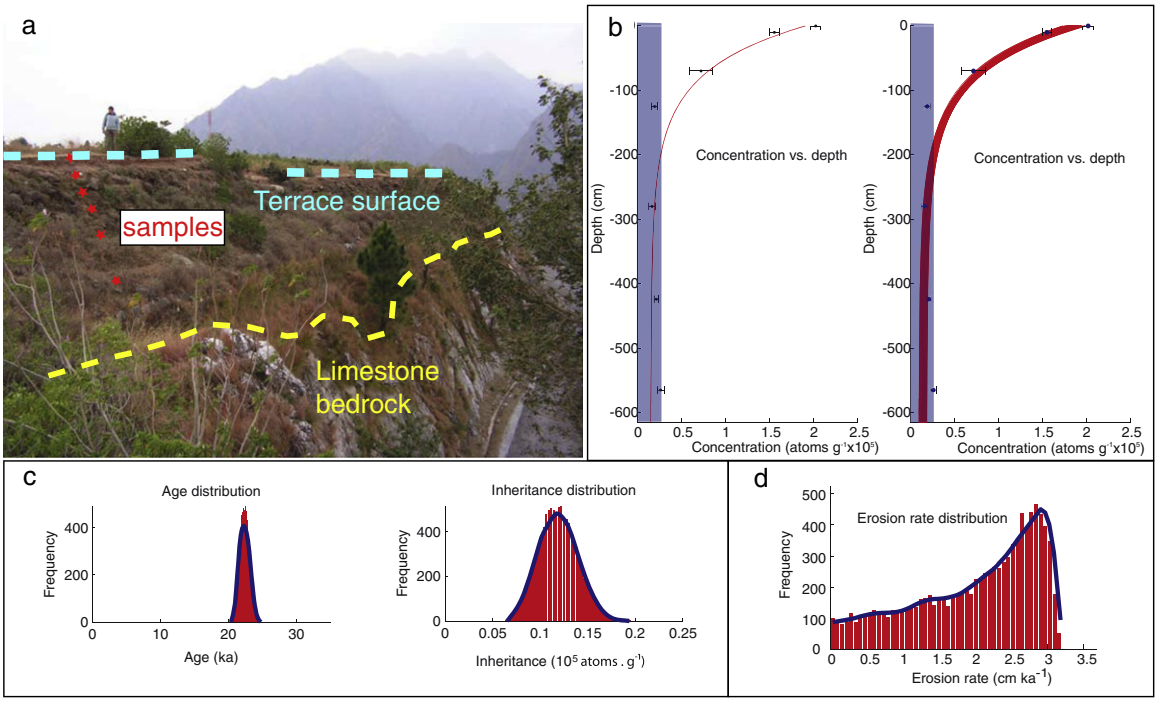

Fig. 8. (a) TCN sampling site for HzeroC terrace. (b): TCN concentration versus depth for the HzeroC samples and modelling attenuation (red lines) for an erosion assumed to be zero; (right) calculated solutions for χ^2 limited to 15; (left) best fit (minimum $\chi^2 = 12$) between the model and sample distribution; the blue box corresponds to the allowed inheritance range. (c) Statistical distribution of the ages and inheritance calculated with the erosion assumed to be zero and the χ^2 limited to 15. (d) Statistical distribution of the erosion rates and age of HzeroC when the erosion rates are not limited.

and growth curves are shown in the online Supplementary material, Appendix 2. A detailed analysis of the curves shows that: a) all the shine-down curves deplete very fast and indicate that the signal solely comes from quartz, a necessary condition for the SAR procedures (Murray and Wintle, 2000); b) a few aliquots show a dose recycling ratio greater than 10% and have been excluded; c) a large dispersion of the aliquot palaeodoses is found in all samples and the youngest OSL ages (Table 2), calculated from the median of the lower 20% of the

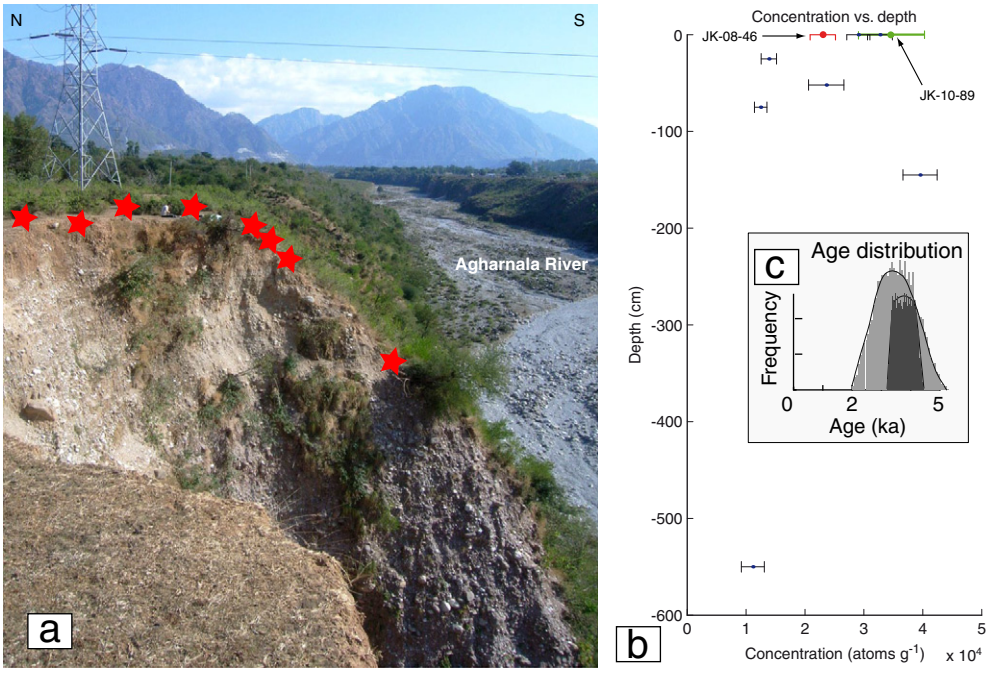

Fig. 9. (a) Picture of the F2AC sampling site; red stars for sample locations. (b) TCN concentration versus depth for the F2AC samples; the red surface sample (JK-08-46) is the sample used to date F2AC. The green surface sample (JK-10-89) is from the Nodda F2NC surface for comparison with the F2AC surface samples; (c) Age distribution obtained for samples JK-08-46 (terrace F2AC in heavy grey) and JK-10-89 (terrace F2NC in light grey).

Table 2
Location, U-Th-K concentrations, dosimetry, palaeodoses, and ages of the OSL samples.

Units		FzeroC	FzeroNC	FH1N (base)	H1N (top)	HzeroC
Location		Footwall of Tea fault	Hangingwall of Tea fault	Footwall of Scorpion fault	Fan apex	Highest terrace
Samples		JK-10-31	JK-10-32	JK-10-33	JK-10-80	K2-12
Lab. number		LD-725	LD-726	LD-727	LD-729	LD-1245
Latitude (°)		33.113	33.113	33.113	33.112	33.121844
Longitude (°)		74.826	74.8256	74.826	74.843	74.816942
Altitude (m)		500	500	500	720	762
Depth from top of unit (m)		25	4	55	6	2
U (ppm)		1.9	1.9	1.5	1.7	2.7
Th (ppm)		14	11.4	7.7	13.6	16.6
K (%)		2.3	1.8	1.9	2.1	1.7
Dose rate (Gy/ka)		3.5 ± 0.2	2.9 ± 0.2	2.7 ± 0.2	3.3 ± 0.2	3.3 ± 0.1
Palaeodose (Gy)	Mean[a]	155 ± 23	129 ± 21	66 ± 26	58 ± 7	151 ± 23
	Least[b]	132 ± 7	104 ± 5	36 ± 4	49 ± 2	120 ± 15
Age (ka)	Mean	44 ± 7	45 ± 8	24 ± 10	18 ± 2	46 ± 7
	Least	38 ± 3	36 ± 3	14 ± 2	15 ± 1	36 ± 5

[a] The single-aliquot regeneration protocol (SAR, from Murray and Wintle, 2000) on ~30 aliquots was used to estimate the mean palaeodose; all aliquots with recycle ratios within 10% are considered.
[b] The least palaeodose consists of the median of the lower 20% of the palaeodoses (see online Supplementary material, Appendix 3 for the palaeodose distribution, shine-down curves and growth curves).

palaeodoses, are considered in the following as more robust than the mean ages (see Section 2.2.2 and the discussion in the online Supplementary material, Appendix 2), an assumption already made by Srivastava et al. (2013a,b) and Mehta et al. (2014). The youngest OSL ages and their geological background are presented below.

4.2.1. The lower units (FzeroC and FzeroNC)

Two samples (samples JK-10-31 and JK-10-32, Table 2) were collected from sand banks in the FzeroC and FzeroNC deposits (Fig. 4d). The youngest OSL ages are 38 ± 3 and 36 ± 3 ka, respectively. They suggest similar ages for the FzeroC and FzeroNC units and a high sedimentation rate at that time. Nonetheless, the development of the erosional surface in the hangingwall of the Tea fault indicates that the footwall sedimentation rate was momentarily smaller than the vertical throw rate along this fault (i.e. smaller than ~10 mm/yr; see Section 5.2).

4.2.2. The Nodda fan (F1N and H1N)

Two samples (samples JK-10-33 and JK-10-80, Table 2) were collected from the Nodda sediments: one from the base of F1N deposits and one from the top of H1N deposits at the apex of the fan (Fig. 3b). Their youngest OSL ages are 14 ± 2 and 15 ± 1 ka, respectively. These two ages are not significantly different and confirm that the two F1N and H1N units are the upstream and downstream parts of a single fan. The apparent reversal of the stratigraphic order between the two ages is either due to measurement uncertainty or is linked to the development of the fan by a progradation where the youngest deposits are located downstream. In this latter case, the fan would have been deposited over a period of less than 4000 years.

4.2.3. The upper terrace (HzeroC)

One sample (samples K2-12, Table 2) was collected 2 m beneath the surface of HzeroC. The youngest OSL age is 36 ± 5 ka. The youngest OSL age of HzeroC is the same as the youngest OSL ages for the lower units of the footwall (FzeroC and FHzeroNC). These numeric ages therefore suggest a correlation between HzeroC, FzeroC and FHzeroNC.

4.3. Comparison between the OSL and TCN ages

Sampling was initially performed in order to compare the OSL ages with the TCN ages for all the major terrace levels. Unfortunately, several samples were not analysed for various reasons and several TCN analyses did not furnish ages mostly due to the presence of an impurity in the quartz grains. Hence, only the upper terrace HzeroC was dated by two methods (i.e. OSL and TCN). The minimum ^{10}Be age (23 ka) estimated for sample JK.08.15, assuming no erosion, is very different from the mean OSL age (46 ± 7 ka) of sample K2–12; the youngest OSL age (36 ± 5 ka) is in agreement with the median ^{10}Be age (37 ka) provided by Hidy et al.'s (2010) analysis of the vertical profile (samples JK.08.03 to JK.08.15). We do not believe that the small difference between these two numerical ages reflects the precision of the two methods, but these comparisons suggest that erosion has to be taken into account through ^{10}Be depth profile studies and that the youngest OSL age is more robust than the mean OSL age to estimate the age of the sediments in Himalayan rivers.

5. Discussion

5.1. Geomorphological evolution of the Riasi area

5.1.1. Summary of the geomorphological study

From the above analysis, 23 sedimentary units are defined from their lower and upper boundaries (Table 3). The relationships between all these units are summarized in Fig. 10a. Eleven units are numerically dated: three units by TCN, four units by OSL, one unit by combined dating using OSL and TCN, whereas the numerical ages of three units are based on previous works (Hebeler et al., 2010; Vignon, 2011; Vassallo et al., 2015). From geometric arguments, three other units correlate to numerically dated levels.

Two major allostratigraphic units, which extended simultaneously above the hangingwall and the footwall, are defined with upper surface ages estimated at ~15 and ~36 ka (right side of Fig. 10a). The HzeroC, FzeroC and FzeroNC units are parts of a same allostratigraphic unit deposited around 36 ka based on OSL and ^{10}Be datings. The H1C and F1N units were deposited simultaneously as the latter provided a youngest OSL age of ~15 ka whereas the former has a maximum age of 15.4 ka from the ^{10}Be age inferred above. It is worth noting that the two allostratigraphic units are encased terraces in the hangingwall but superposed sedimentary units in the footwall.

Two other units could be correlated between the hangingwall and footwall (H4 to F3 and H5 to F4 respectively). Two units were only found in the hangingwall (H0bis and H2C) and one other only in the footwall (F5).

The elevation distribution of these units is analysed below, in order to quantify the incision rates and to specify the climatic and tectonic controls.

5.1.2. Local palaeogeographic variations

The allostratigraphic unit comprised of the HzeroC and FzeroC units deposited in a palaeogeographic setting where the Chenab River was flowing southward before ~36 ka (Fig. 11). After ~36 ka, the channel

Table 3
List and characteristics of the sedimentary units. Estimation of the ages: *from the youngest OSL age; $from TCN; *$from TCN and OSL (uncertainties from the youngest OSL age); £from ^{14}C; [1]from Vignon (2011) and Vassallo et al. (2015); [2]from Hebeler et al. (2010); [?]from the lateral correlation or encased relationships.

Name	Structural location	Geographic location	Origin of the sediment	Thickness max (m)	Upper boundary	Lower boundary	Age (ka)
HzeroC	Hangingwall	Left side Chenab	Chenab River	15 m	Surface	Limestone	*$36 ± 5
HzeroCbis	Hangingwall Riasi thrust	Left side Chenab	Chenab River	10 m	Surface	Limestone	36 > ? > 15
H1C	Hangingwall Riasi thrust	Left side Chenab	Chenab River	15 m	Surface	Limestone	$7–16
H2C	Hangingwall Riasi thrust	Left side Chenab	Chenab River	8 m	Surface	Limestone	14 > ? > 4
H3C	Hangingwall Riasi thrust	Left side Chenab	Chenab River	15 m	Surface	Limestone	?~4
H4C	Hangingwall Riasi thrust	Left side Chenab	Chenab River	6 m	Surface	Limestone	?<4
H5C	Hangingwall Riasi thrust	Left side Chenab	Chenab River	?	Surface	Limestone	?<4
H1N	Hangingwall Pilar fault	Left side Nodda	Nodda River	25 m	Surface	Limestone	*15 ± 1
FzeroNC	Footwall Spring fault	Left and right sides Nodda	Nodda and Chenab	12 m	F1N unit	Limestone, FzeroC	*38 ± 3
FzeroC	Footwall Riasi Thrust	Left and right sides Nodda	Chenab River	21 m	FzeroNC	Siwalik	*36 ± 3
F1N	Footwall Pilar fault	Left and right sides Nodda	Nodda River	60 m	Surface	FzeroNC	*14 ± 2
F1A	Footwall Riasi Thrust	Right side Anji	Anji River	61 m	Surface	?	?~15
F1C	Above frontal anticline	Left sides Chenab and Anji	Chenab River	10 m	Surface	Siwalik	$[1]13–21
F2C	Above frontal anticline	Left sides Chenab and Anji	Chenab River	10 m	Surface	Siwalik	$[1]3.2–6.9
F2N	Footwall Riasi fault	Left and right sides Nodda	Nodda River	4 m	Surface	F1N	£[2]~4
F2NC	Footwall Riasi fault	Left side Chenab, both side Nodda	Nodda and Chenab	4 m	Surface	F1N	$2–5.3
F2AC	Footwall Riasi fault	Left side Chenab, right side Anji	Anji and Chenab	6 m	Surface	F1A	$3.2–4.3
F2C	Footwall Pilar fault	Right side Chenab	Chenab River	8 m	Surface	Limestone, Quaternary	?~4
F2A	Footwall Riasi fault	Right side Anji	Anji River	4 m	Surface	Siwalik or F1A	?~4
F3C	Footwall Riasi fault	Left side Chenab, right side Anji	Chenab River	7 m	Surface	Siwalik	?<4
F4C	Footwall Riasi fault	Left side Chenab	Chenab River	7 m	Surface	Siwalik or F1A	?<4
F5AC	Footwall Riasi fault	Left side Chenab, right side Anji	Chenab River	8 m	Surface	Siwalik or F1A	?<4
F5A	Footwall Riasi fault	Left side Nodda	Anji River	?	Surface	?	?<4

of the Chenab River moved toward the west and this lateral motion allows units HzeroC to H5Cto be preserved from erosion.

The H1N fan deposited after the HzeroCbis terrace, but its apex was nearly at the same altitude as the already uplifted HzeroCbis terrace, due to the steeper river slope of the Nodda River with respect to the Chenab River.

5.1.3. Base level variations

Base level variations of a river are deduced from the incision and sedimentation in the footwall of a thrust (Section 2.1) and are expressed relative to a reference point located in the substratum of the footwall. From the comparison of the above sedimentological, geomorphological and chronological results, the variation in incision and sedimentation is subdivided into six major stages at the footwall of the Riasi thrust (Fig. 10b, stages **1** to **6**): - **1)** FzeroC and FzeroNC units were deposited ~36 ka ago and have a total thickness of 37 m. Taking into account the age estimation of the OSL samples located close to the top and the base of the unit, the level of the Chenab River increased by ~37 m in less than 8000 years; - **2)** No erosion surface is found between the FzeroNC and F1N units, suggesting a steady-state base level during the 36 to ~15 ka period; - **3)** Before ~14 ka, F1N and F1A fans were deposited along the tributaries. The aggradation, which reached 61 m close to the boundary between the Nodda fan and Chenab palaeo-river, was driven by an increase in the Chenab River level in respect to the footwall substratum. The OSL ages of the two samples located close to the top and the base of the Nodda fan are not significantly different and suggest that the sedimentation rate was very high; - **4)** Between 14 and 4 ka, the vertical erosion rate is low (in the order of 1 mm/yr from the height of the fluvial scarp between the F1 and F2 levels); - **5)** The strath or fill-cut terraces (F2N, F2NC, F2AC, F2C) were formed between 5.3 and 3.8 ka from the TCN dating of the F2AC and F2NC surfaces, and were linked to a lateral erosional event during a stage of nearly steady base level; - **6)** Since ~4 ka, a major vertical incision has been occurring and the mean footwall incision rate has reached 12 mm/yr.

5.2. Tectonics deduced from footwall and hangingwall incisions

In order to calculate the vertical throw of the thrust, the observed incisions are compared using a reference point. This reference is chosen at the intersection, ~36 ka ago, between the MWT and the right bank of the Chenab River (black dot on Fig. 11), a choice that minimizes the influence of the Chenab meander evolution because the reference is presently still located close to the Chenab River, but on its present-day left side. It is also assumed that the N–S slope of the Chenab River did not vary over time between the present-day confluence of the two rivers and the reference point. Furthermore the tectonic effects of the Rain and Scorpion faults are removed, on the basis of their scarp height at the top of the Nodda fan (Vignon, 2011; Mugnier et al., in press) in order to restore the initial height of the FzeroC and FzeroNC units with respect to the reference point.

The vertical throw of a fault (V; Fig. 10c) is deduced from the incision (I;Fig. 10B) by using Eq. (6). The two allostratigraphic units, the surface of which is dated at ~15 and ~36 ka, extended above the hangingwall and footwall of the MWT. They are presently vertically offset by the MWT by 190 and 375 m, respectively.

HzeroC, H1C, and H3C are three thick units deposited in the hangingwall of the Riasi thrust and are parts of allostatigraphic units that also extended at the footwall because they occurred when the sedimentation rate at the footwall was greater than the tectonic uplift. The footwall twins of the FzeroC and H1C units are recognized above based on numerical dating; it is suggested that H3C should be correlated with the level largely expressed at the footwall (F2N, F2NC, F2AC, and F2C) and dated by TSL between 5.3 and 3.8 ka; in this case, the vertical offset would be 50 m.

The incision rate of the hangingwall varies between 25 and 6.5 mm/yr for the three periods defined by these allostatigraphic units (Fig. 10b). The vertical throw rate during the same three periods only varies between 13 and 9 mm/yr (Fig. 10c) and remains similar to the mean throw rate during the last 36 ka (10.6 ± 2 mm/yr). This result is close to the 9.3 ± 2 mm/yr mean throw rate inferred for the last 15 ka from other studies (Vassallo et al., 2015; Mugnier et al., in press) that consider the Nodda fan (H1N and F1N) as a passive marker. The good fit found between the two approaches lends weight to the 11.2 ± 3.8 mm/yr shortening rate estimate of Vassallo et al. (2015) with respect to the smaller estimate (6–7 mm/yr) proposed by Gavillot et al. (2016).

In summary, the MWT is growing regularly with a vertical throw rate close to 10 mm/yr and no tectonic fluctuations punctuate the development of the main sedimentary units since at least a few thousand years. The latter are only passively offset by the fault. Nonetheless, Mugnier et al. (2005) and Bollinger et al. (2014) have shown that the abandonment of some small-scale terraces at the hangingwall of the MFT was linked to the great earthquakes that reached the front.

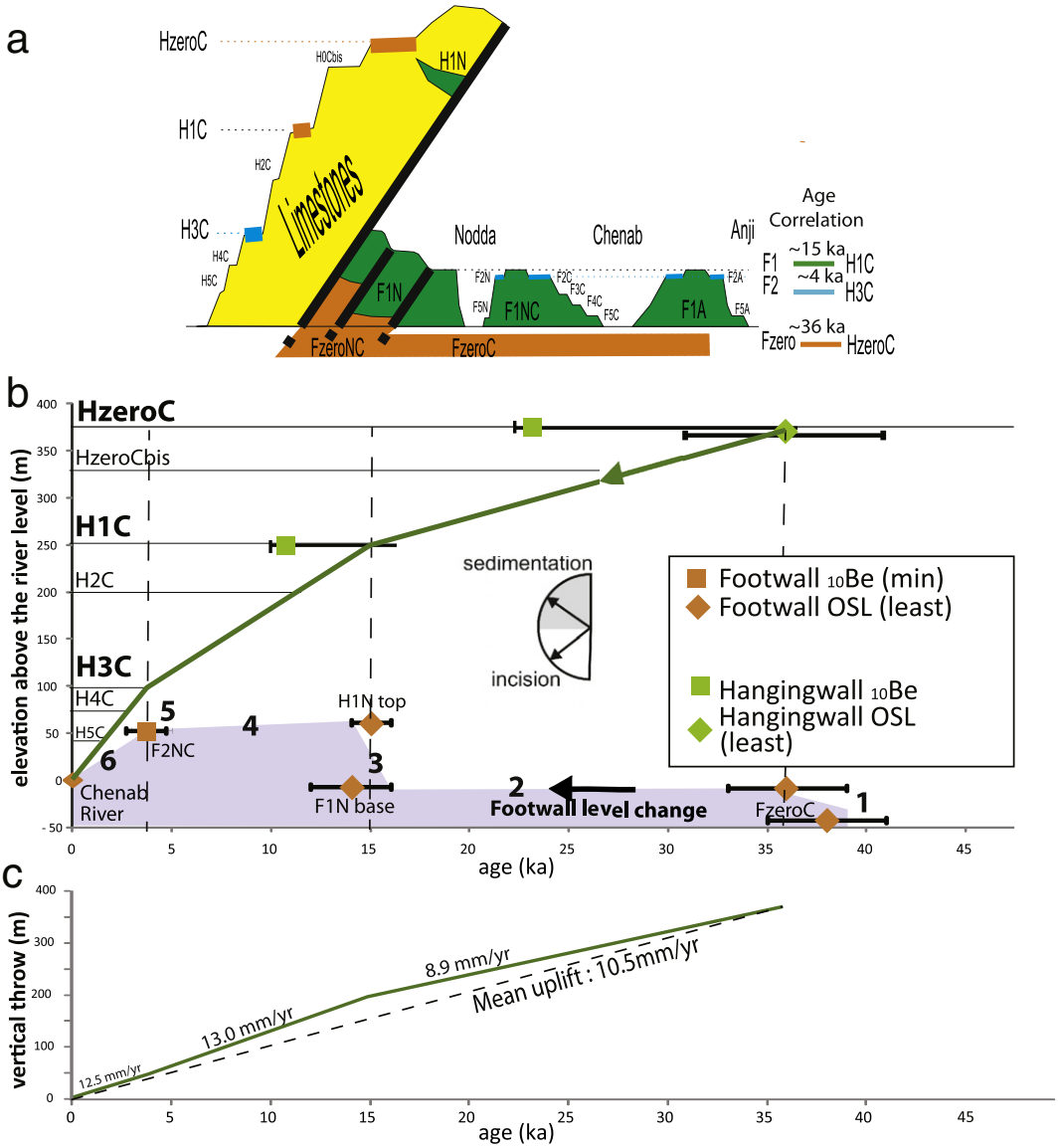

Fig. 10. (a) Sketch of the relationships between the terraces and allostratigraphic units. (b) Elevation of the sedimentary units with respect to the present-day Chenab River level on both sides of the Riasi fault: green and orange symbols are for the hangingwall terraces and footwall deposits, respectively; squares and diamonds refer to the two types of ages respectively (min. ^{10}Be age assuming no erosion and youngest OSL age); the error bars for the ^{10}Be ages refer to the interval between the peak and the medium value deduced from Hidy et al.'s (2010) approach; the errors estimate for the youngest OSL age is explained in the Supplementary material, Appendix 3. (c) Difference in elevation between the hangingwall and footwall of the allostratigraphic units as a function of time; from Eq. (6), this difference is the vertical throw of the Riasi thrust zone.

Therefore, some of the small strath levels in the hangingwall of the MWT (H2C, H0Cbis) could be related to the instantaneous uplift linked to an earthquake slip on the fault and to the following vertical incision.

5.3. Regional climate variations

The aggradation/incision events observed in Riasi area do not coincide with the changes in the tectonic velocity of the MWT, but are synchronous with climatic events already found in Himalaya:

Stages -1 and -3 of the base level changes (Fig. 10b) are synchronous with the ~36 and ~14–15 ka aggradation events in Western Himalaya (Bookhagen et al., 2006; Dortch et al., 2011). Similar aggradation phases also occurred between 38 and 35 ka in Central Himalaya (Pratt-Sitaula et al., 2004) and between 18 and 11 ka along the Ganga River (Ray and Srivastava, 2010). They were also recorded in the inner belt of Pir Panjal (Vignon, 2011; Vignon et al., 2014; Vassallo et al., 2015).

The ~4 ka lateral incision of stage 5 in the Riasi area also occurred in the upper catchments of the tributaries of the Chenab River (Vassallo et al., 2015).

Fluvial incision reflects changes in the monsoon intensity and deglaciation events in Himalaya (e.g. Dortch et al., 2011). A dry condition generally leads to a decrease in the stream power (e.g. Bookhagen et al., 2005) whereas an intensified monsoon phase (Bookhagen et al., 2006) increases the transport capacity. The 36 and ~14–15 ka aggradation events in Western Himalaya were related to the end of the intensified monsoon phases (Bookhagen et al., 2006; Dortch et al., 2011) whereas the ~4 ka event was synchronous with dry conditions described in the lakes of the High Himalaya (Ambili, 2013) and Jammu areas (Trivedi et al., 2013). Therefore, the episodic fluvial aggradation/

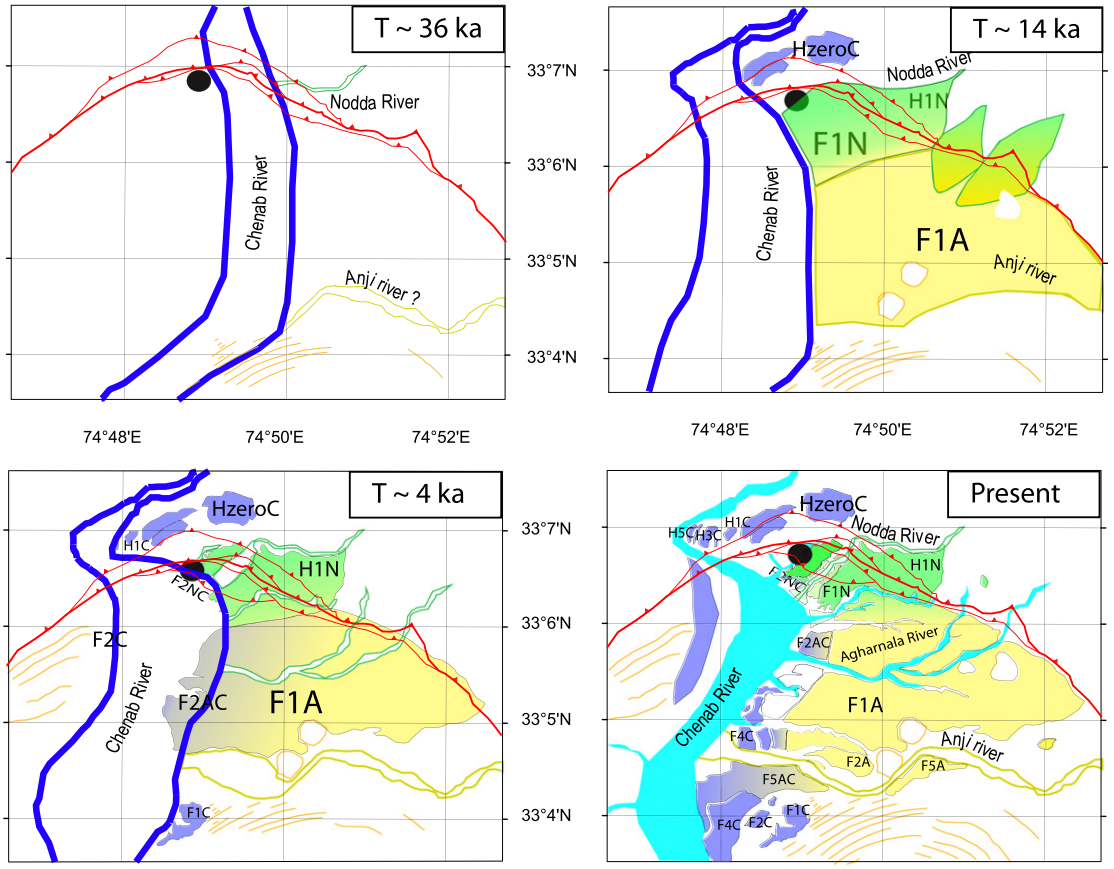

Fig. 11. Evolution of the river pattern in the Riasi area since ~36 ka. The Chenab River is represented in blue, the Nodda River in green and the Anji River in yellow. Terraces have the same colour code. The black dot refers to the incision reference point.

incision events observed at the footwall of the Riasi thrust are most likely driven by climatic fluctuations in Himalaya.

6. Conclusion

Tectonics and fluvial base level changes have been estimated at the vicinity of an out-of-sequence thrust by using a strategy that takes into account: a) the structural location of the sedimentary units; b) a relative chronology that includes both the cut and fill history of the sedimentary units; c) their numerical dating by OSL and ^{10}Be cosmogenic isotopes; and d) precise topographic measurements. This geomorphic and sedimentological study has been performed at the intersection between the Chenab River and the Medlicott-Wadia Thrust (MWT). It has enabled us to correlate strath terraces developed in the hangingwall to several ten meter thick sedimentary units in the footwall.

The numeric ages of the three major allostratigraphic units (Fzero F1, and F2) were calculated from the analysis of 19 ^{10}Be samples and five OSL samples. The ages are estimated at 36 ± 3, ~15, and ~4 ka. We showed evidence of two phases of sedimentation at ~36–38 and 14–15 ka associated with 30 and 75 m thick sedimentary units respectively, and a phase of lateral incision at ~4 ka that produced a strath terrace. Two other units can be geometrically correlated between the hangingwall and footwall whereas other units were only locally found in either the hangingwall or footwall.

The vertical throw rate of the MWT is calculated by taking the relative base level fluctuations into account; we found an incision rate in the hangingwall that varied from 25 to 6.5 mm/yr but a constant vertical throw rate of 10.6 ± 2 mm/yr since ~36 ka. The high value for the displacement rate along the MWT suggests that a large number of earthquakes occurred along this out-of-sequence thrust and that the 2005 Kashmir earthquake was one amongst them. Although the slip cyclically occurs during earthquakes, our results imply a regular growing of the MWT at the scale of several thousands of years.

The tectonics of the frontal structure does not punctuate the development of the sedimentary units at its back and his structure is probably growing regularly at the scale of a few thousand years. The three major aggradation/incision events observed in the Riasi area are most likely driven by climatic fluctuations, as already observed elsewhere in Himalaya; the other units, of local importance, could either be linked to local lateral incision during extreme flooding and/or to an increase in the vertical incision after an earthquake-related uplift.

Therefore, the short-term cyclic seismic component of displacement does not significantly affect the development of large-scale terraces. The rhythm of the sedimentary record in a mountain belt appears to be mainly controlled by the climatically-driven base level changes; the long-term tectonics is more regular and do not induce cyclic sedimentary events.

Acknowledgments

This research was funded by the programs of the ANR (n° ANR-06-CATT-007 PAKSIS), INSU, and Labex@OSUG 2020 (Govt of France).

RJ kindly acknowledges the financial support from MoES Project (vide # MoES/P.O.(Seismo)/1/(175)/2013, dated 19/6/14. Govt. of India). RJ and PS also acknowledge partial support from the WIHG Project under the MOU between WIHG and U. Savoy Mont Blanc.

RJ and PS would like to sincerely thank the Director, WIHG. Thank you also to R. Thiede, G. Mascle, A. Plater, C. Sutcliffe and S. Mullin who carefully reviewed the manuscript.

Appendix A. Supplementary data

Supplementary data to this article can be found online at http://dx.doi.org/10.1016/j.geomorph.2016.07.040.

References

Aitken, M.J., 1998. An Introduction to Optical Dating. Oxford University Press, Oxford (280 pp.).

Allen, P., 2005. Striking a chord. Nature 434 (7036), 961.

Ambili, A., 2013. Lake Sediments as Climate and Tectonic Archives in the Indian Summer Monsoon Domain. (PhD university of Potsdam, 141 pp. http://opus.kobv.de/ubp/volltexte/2013/6479/).

Ambraseys, N.N., Douglas, J., 2004. Magnitude calibration of north Indian earthquakes. Geophys. J. Int. 159 (1), 165–206.

Anderson, R.S., Repka, J.L., Dick, G.S., 1996. Explicit treatment of inheritance in dating depositional surfaces using in situ ^{10}Be and ^{26}Al. Geology 24 (1), 47–51.

Arnold, M., Merchel, S., Bourles, D., Braucher, R., Benedetti, L., Finkel, R., Aumaitre, G., Gottdang, A., Klein, M., 2010. The French accelerator mass spectrometry facility ASTER: improved performance and developments. Nucl. Instrum. Methods Phys. Res., Sect. B 268 (11−12), 1954–1959.

Balco, G., Stone, J.O., Lifton, N.A., Dunai, T.J., 2008. A complete and easily accessible means of calculating surface exposure ages or erosion rates from ^{10}Be and ^{26}Al measurements. Quat. Geochronol. 3, 174–195.

Bierman, P.R., Gillespie, A.R., Caffee, M.W., 1995. Cosmogenic ages for earthquake recurrence intervals and debris flow fan deposition, Owens Valley, California. Science 270 (5235), 447–450.

Bollinger, L., Sapkota, S.N., Tapponnier, P., Klinger, Y., Rizza, M., Van der Woerd, J., Tiwari, D.R., Pandey, R., Bitri, A., Bes de Berc, S., 2014. Estimating the return times of great Himalayan earthquakes in eastern Nepal: evidence from the Patu and Bardibas strands of the Main Frontal Thrust. J. Geophys. Res. Solid Earth http://dx.doi.org/10.1002/2014JB010970.

Bookhagen, B., Thiede, R.C., Strecker, M.R., 2005. Late Quaternary intensified monsoon phases control landscape evolution in the northwest Himalaya. Geology 33 (2), 149–152.

Bookhagen, B., Fleitmann, D., Nishiizumi, K., Strecker, M.R., Thiede, R.C., 2006. Holocene monsoonal dynamics and fluvial terrace formation in the northwest Himalaya, India. Geology 34 (7), 601–604.

Braucher, R., Brown, E., Bourlès, D., Colin, F., 2003. In situ produced ^{10}Be measurements at great depths: implications for production rates by fast muons. Earth Planet. Sci. Lett. 211 (3), 251–258.

Brown, E.T., Edmond, J.M., Raisbeck, G.M., Yiou, F., Kurz, M.D., Brook, E.J., 1991. Examination of surface exposure ages of Antarctic moraines using in situ produced ^{10}Be and ^{26}Al. Geochim. Cosmochim. Acta 55 (8), 2269–2283.

Brown, E.T., Stallard, R., Larsen, L., Raisbeck, G.M., Yiou, M., 1995. Denudation rates determined from the accumulation of in situ-produced ^{10}Be in the luquillo experimental forest, Puerto Rico. Earth Planet. Sci. Lett. 129 (1–4), 193–202.

Brown, E.T., Bourlés, D., Raisbeck, G.M., Yiou, F., Burchfiel, B.C., Molnar, P., Qidong, D., Jun, L., 1998. Estimation of slip rates in the southern Tien Shan using cosmic ray exposure dates of abandoned alluvial fans. Geol. Soc. Am. Bull. 110 (3), 377–386.

Burbank, D.W., Anderson, R., 2001. Tectonic Geomorphology. Blackwell Publishing, Malden, MA 0-632-04386-5.

Castelltort, S., Whittakeret, A., Vergés, J., 2015. Tectonics, sedimentation and surface processes: from the erosional engine to basin deposition: tectonics, sedimentation and surface processes. Earth Surf. Process Landforms http://dx.doi.org/10.1002/esp.3769.

Chmeleff, J., von Blanckenburg, F., Kossert, K., Jakob, J., 2010. Determination of the ^{10}Be half-life by multicollector ICP-MS and liquid scintillation counting. Nucl. Inst. Methods Phys. Res. B 268 (2), 192–199.

Dortch, J.M., Owen, L.A., Dietsch, C., Caffee, M.W., Bovard, K., 2011. Episodic fluvial incision of rivers and rock uplift in the Himalaya and Transhimalaya. J. Geol. Soc. Lond. 168, 783–804. http://dx.doi.org/10.1144/0016-76492009-158.

Duller, G.A.T., 2007. Analyst. Manual, pp. 1–45.

Dunne, J., Elmore, D., Muzikar, P., 1999. Scaling factors for the rates of production of cosmogenic nuclides for geometric shielding and attenuation at depth on sloped surfaces. Geomorphology 27, 3–11.

Frankel, K.L., Finkel, R., Owen, L., 2011. Terrestrial cosmogenic nuclide geochronology data reporting standards needed. Eos Trans. Am. Geophys. Union 91 (4), 31–32.

Galbraith, R.F., Roberts, R.G., Laslett, G.M., Yoshida, H., Olley, J.M., 1999. Optical dating of single and multiple grains of quartz from Jinmium rock shelter, Northern Australia: part I, experimental design and statistical models. Archaeometry 41, 338–364.

Gansser, A., 1964. Geology of the Himalayas. Inter science publishers, John Wiley & Sons (289 pp.).

Gavillot, Y., Meigs, A., Yule, D., Heermance, R., Rittenour, T., Madugo, C., Malik, M., 2016. Shortening rate and Holocene surface rupture on the Riasi fault system in the Kashmir Himalaya: active thrusting within the Northwest Himalayan orogenic wedge. Geol. Soc. Am. Bull. http://dx.doi.org/10.1130/B31281.1.

Hancock, G.S., Anderson, R.S., Chadwick, O.A., Finkel, R.C., 1999. Dating fluvial terraces using ^{10}Be and ^{26}Al profiles: application to the Wind River, Wyoming. Geomorphology 27, 41–60.

Hebeler, A., Madden, C., Malik, M.A., Kaericher, M., Gavillot, Y., Yule, D., Meigs, A., 2010. Middle Holocene surface rupture of the Riasi thrust, Kashmir, India. Annual Meeting of the Seismological Society of America, Portland, OR, 21–23 April.

Hetzel, R., Niedermann, S., Tao, M., Kubik, P.W., Ivy-Ochs, S., Gao, B., Strecker, M.R., 2002. Low slip rates and long-term preservation of geomorphic features in Central Asia. Nature 417, 428–432.

Hidy, A.J., Gosse, J.C., Pederson, J.L., Mattern, J.P., Finkel, R.C., 2010. A geologically constrained Monte Carlo approach to modeling exposure ages from profiles of cosmogenic nuclides: an example from Lees Ferry, Arizona. Geochem. Geophys. Geosyst. 11, 18.

Hughes, P.D., 2010. Geomorphology and Quaternary stratigraphy: the roles of morpho-, litho-, and allostratigraphy. Geomorphology 123, 189–199.

Hussain, A., Yeats, R., MonaLisa, H., 2009. Geological setting of the 8 October 2005 Kashmir earthquake. J. Seismol. 13 (3), 315–325.

Huyghe, P., Mugnier, J.L., 1994. Basins inversions and paleostress: an example from the southern North Sea. In: Roure, F. (Ed.), Peri-Tethyan Plateforms. Edition Technips, pp. 211–229.

Jayangondaperumal, R., Mugnier, J.L., Dubey, A.K., 2013. Earthquake slip estimation from the scarp geometry of Himalayan Frontal Thrust, western Himalaya: implications for seismic hazard assessment. Int. J. Earth Sci. (Geol. Rundsch.) 102, 1937–1955.

Johnson, G., Johnson, N., Opdyke, N., Tahirkheli, R., 1979. Magnetic reversal stratigraphy and sedimentary tectonic history of the Upper Siwalik Group, Eastern Salt Range and southwestern Kashmir. In: Farah, A., DeJong, K. (Eds.), Geodynamics of Pakistan. Geological Survey of Pakistan, Quetta, pp. 149–165.

Jouanne, F., Awan, A., Pêcher, A., Kausar, A., Mugnier, J.L., Khan, I., Khan, N.A., Van Melle, J., 2014. Present-day deformation of the northwestern Himalaya. J. Geophys. Res. Solid Earth 119 (3), 2487–2503.

Kaneda, H., Nakata, T., et al., 2008. Surface rupture of the 2005 Kashmir, Pakistan, earthquake and its active tectonic implications. Bull. Seismol. Soc. Am. 98 (2), 521–557.

Kirby, E., Whipple, K., 2001. Quantifying differential rock-uplift rates via stream profile analysis. Geology 29 (5), 415–418.

Krishnaswamy, V.S., Jalote, S.P., Shome, S.K., 1970. Recent crustal movements in northwest Himalaya and the Gangetic foredeep and related patterns of seismicity. Symp. Earthquake Eng., 4th Roorkee, pp. 419–439.

Kumar, S., Wesnousky, S., Rockwell, T.K., Briggs, R.W., Thakur, V.C., Jayangondaperumal, R., 2006. Paleoseismic evidence of great surface rupture earthquakes along the Indian Himalaya. J. Geophys. Res. 111 (B3), B03304.

Lal, D., 1991. Cosmic ray labeling of erosion surfaces: in situ nuclide production rates and erosion models. Earth Planet. Sci. Lett. 104 (2–4), 424–439.

Lavé, J., Avouac, J.P., 2001. Fluvial incision and tectonic uplift across the Himalayas of central Nepal. J. Geophys. Res. 106 (B11), 26561–26591.

Marshak, S., 2004. Salients, recesses, arcs, oroclines, and syntaxes; a review of ideas concerning the formation of mapview curves in fold-thrust belts. In: Mc Clay (Ed.), Thrust Tectonics and Hydrocarbon System. A. A. P. G. Mem. 82, pp. 131–156.

Mehta, M., Dobhal, D.P., Pratap, B., Majeed, Z., Gupta, A.K., Srivastava, P., 2014. Late Quaternary glacial advances in the Tons River Valley, Garhwal Himalaya, India and regional synchronicity. Holocene (0959683614540947).

Middleton, R., Brown, L., Dezfouly-Arjomandy, B., Klein, J., 1993. On ^{10}Be standards and the half-life of ^{10}Be. Nucl. Inst. Methods Phys. Res. 82 (3), 399–403.

Mugnier, J.L., Huyghe, P., 2006. The Ganges basin geometry records a pre-15 Ma isostatic rebound of Himalaya. Geology 34 (6), 445–448.

Mugnier, J.-L., Mascle, G., Faucher, T., 1992. La structure des Siwaliks de l'Ouest Népal: un prisme d'accrétion intracontinental. Bull. Soc. Géol. Fr. 163 (5), 585–595.

Mugnier, J.L., Huyghe, P., Gajurel, A., Becel, D., 2005. Frontal and piggy-back seismic ruptures in the external thrust belt of Western Nepal. J. Asian Earth Sci. 25 (5), 707–717.

Mugnier, J.L., Gajurel, A., Huyghe, P., Jayangondaperumal, R., Jouanne, F., Upreti, B., 2013. Structural interpretation of the great earthquakes of the last millennium in Central Himalaya. Earth Sci. Rev. 127, 30–47.

Mugnier, J.L., Vignon, V., Vassallo, R., Malik, M., Jayangondaperumal, R., Srivastava, P., Replumaz, A., Jouanne, F., Buoncristiani, J.F., Jomard, H., Carcaillet, J., 2016. A Complex Thrust Sequence in Western Himalaya: The Active Medlicott Wadia Thrust, Quaternary International (in press).

Murray, A.S., Wintle, A.G., 2000. Luminescence dating of quartz using improved single-aliquot regenerative-dose protocol. Radiat. Meas. 32, 57–73.

Nawani, P.C., Khan, S., Singh, O., 1982. Geologic-cum geomorphic evolution of the western part of Chenab basin with special reference to Quaternary tectonics. Himal. Geol. 12, 18.

Nissen, E., Walker, R., Molor, E., Fattahi, M., 2009. Late Quaternary rates of uplift and shortening at Baatar Hyarhan (Mongolian Altai) with optically stimulated luminescence. Geophys. J. Int. 177, 259–278.

Pêcher, A., Seeber, L., Guillot, S.,,F., Jouanne, F., Kausar, A., Latif, M., Majid, A., Mahéo, G., Mugnier, J.L., Rolland, Y., van der Beek, P., Van Melle, J., 2008. Stress field evolution in the northwest Himalayan syntaxis, northern Pakistan. Tectonics 27 (6), TC6005.

Pratt-Sitaula, B., Burbank, D., Heimsath, A., Qjha, T., 2004. Landscape disequilibrium on 1000–10,000 year scales Marsyandi River, Nepal, central Himalaya. Geomorphology 58 (1–4), 223–241.

Ray, Y., Srivastava, P., 2010. Widespread aggradation in the mountainous catchment of the Alaknanda-Ganga River System: timescales and implications to Hinterland-foreland relationships. Quat. Sci. Rev. 29 (17–18), 2238–2260.

Seeber, L., Armburster, J., 1981. Great detachment earthquakes along the Himalayan arc and long term forecast. In: Sibson, D.W., Richards, P.G. (Eds.), Earthquake Prediction: An International ReviewMaurice Ewing Series 4. Amer. Geophysical Union, Washington D.C., pp. 259–277.

Simpson, G., Castelltort, S., 2012. Model shows that rivers transmit high-frequency climate cycles to the sedimentary record. Geology http://dx.doi.org/10.1130/G33451.1.

Srivastava, P., Bhakuni, S., Luirei, K., Misra, D., 2009. Morpho-sedimentary records at the Brahmaputra River exit, NE Himalaya: climate–tectonic interplay during the Late Pleistocene–Holocene. J. Quat. Sci. 24 (2), 175–188.

Srivastava, P., Kumar, A., Mishra, A., Meena, N.K., Tripathi, J.K., Sundriyal, Y.P., Agnihotri, R., Gupta, A.K., 2013a. Early Holocene monsoonal fluctuations in the Garhwal higher Himalaya as inferred from multi-proxy data from the Malari paleolake. Quat. Res. 80, 447–458.

Srivastava, P., Ray, Y., Phartiyal, B., Sharma, A., 2013b. Late Pleistocene-Holocene morphosedimentary architecture, Spiti River, arid higher Himalaya. Int. J. Earth Sci. 102 (7), 1967–1984.

Stone, J.O., 2000. Air pressure and cosmogenic isotope production. J. Geophys. Res. 105 (B10), 23753–23759.

Thakur, V.C., Jayangondaperumal, R., 2015. Seismogenic active fault zone between 2005 Kashmir and 1905 Kangra earthquake meizoseismal regions and earthquake hazard in eastern Kashmir seismic gap. Curr. Sci. 109 (3), 610–617.

Thakur, V.C., Jayangondaperumal, R., Malik, M., 2010. Redefining Medlicott-Wadia's main boundary fault from Jhelum to Yamuna: an active fault strand of the main boundary thrust in northwest Himalaya. Tectonophysics 489 (1–4), 29–42.

Trivedi, A., Chauman, M.S., Malik, M.A., 2013. Holocene vegetation and climate change in Jammu region, based on pollen evidence from the lake deposits. Man Environ. XXXVIII (1), 74–89.

Vassallo, R., Ritz, J.-F., Carretier, S., 2011. Control of geomorphic processes on ^{10}Be concentrations in individual clasts: complexity of the exposure history in Gobi-Altay range (Mongolia). Geomorphology 135, 35–47. http://dx.doi.org/10.1016/j.geomorph.2011.07.02.

Vassallo, R., Mugnier, J.L., Vignon, V., Malik, M., Jayangondaperumal, R., Srivastava, P., Jouanne, F., Carcaillet, J., 2015. Quaternary deformation and seismic hazard in Northwestern Himalaya. Earth Planet. Sci. Lett. 411, 241–252.

Vergés, J., Burbank, D., Meigs, A., 1996. Unfolding: an inverse approach to fold kinematics. Geology 24 (2), 175–178.

Vignon, V., 2011. Activité hors séquence des chevauchements dans la syntaxe nord- ouest himalayenne: apports de la modélisation analogique et quantification quaternaire par analyse morphotectonique PHD thesis University J. Fourier (278 pp.).

Vignon, V., Srivastava, P., Vassallo, R., Mugnier, J.-L., Carcaillet, J., 2014. Dating of the quaternary terraces close to the Chenab river (Western Himalaya). PANGAEA® Data Publisher for Earth & Environmental Science http://dx.doi.org/10.1594/PANGAEA.836910.

Yanites, B.J., Tucker, G.E., Anderson, R.S., 2009. Numerical and analytical models of cosmogenic radionuclide dynamics in landslide-dominated drainage basins. J. Geophys. Res. 114 (F1), F01007.